DIAGNOSIS AND PROGNOSIS OF DEGRADATION

6.1: Introduction

- Until now, we have focused on developing a single parameterized model that describes a fresh (beginning-of-life) cell and on estimating the cell's internal electrochemical variables using that model.
- In reality, we recognize that a single fixed model may be insufficient:
  - There will be cell-to-cell variations even among fresh cells; also,
  - A cell's characteristics will evolve over time as the cell ages.
- Since a BMS must operate reliably under these conditions, it will need to be able to compensate for variations such as these.
- This chapter focuses on aging-related factors, and how those impact the models we have seen to date.
- The topics leading to this point are foundational; furthermore, the remainder of this course will build on those presented in this chapter.

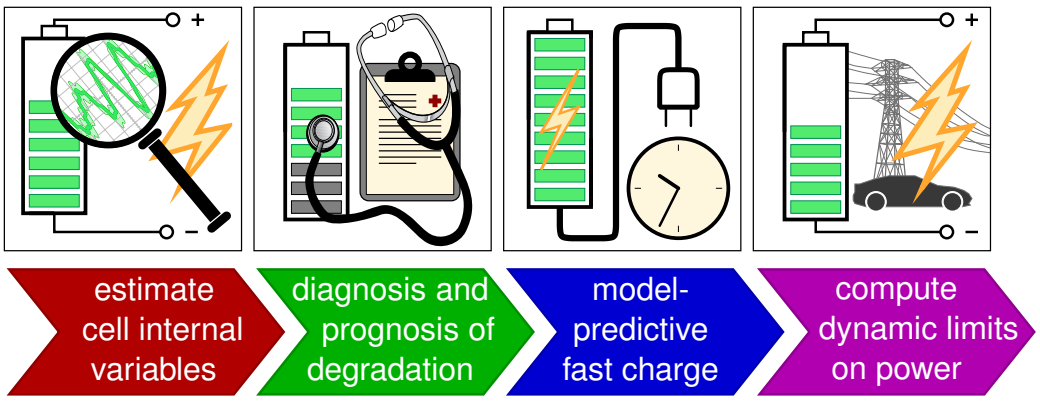

- Future chapters require knowledge on how lithium-ion cells degrade in order to optimize usage to prevent premature aging and failure while still maximizing the performance delivered by the battery pack.
  - In the next topic, we will review cell degradation indicators.
  - We also introduce the concepts of degradation modes versus degradation mechanisms.
- We organize the discussion of a BMS's response to cell aging under the categories of *diagnostics* and *prognostics*.
- These topics of study are still immature and are the focus of many research teams at this point in history.
- We will put forward some preliminary ideas and results, recognizing that there is much work still to do to convert them into mature, robust, and practical real-time methods.

6.2: Degradation indicators, modes, mechanisms

- There are multiple physical processes by which lithium-ion cells are known to degrade; many of these were discussed in ECE5720.
- The figure provides a graphical summary of the primary lithium-ion degradation mechanisms known to exist.

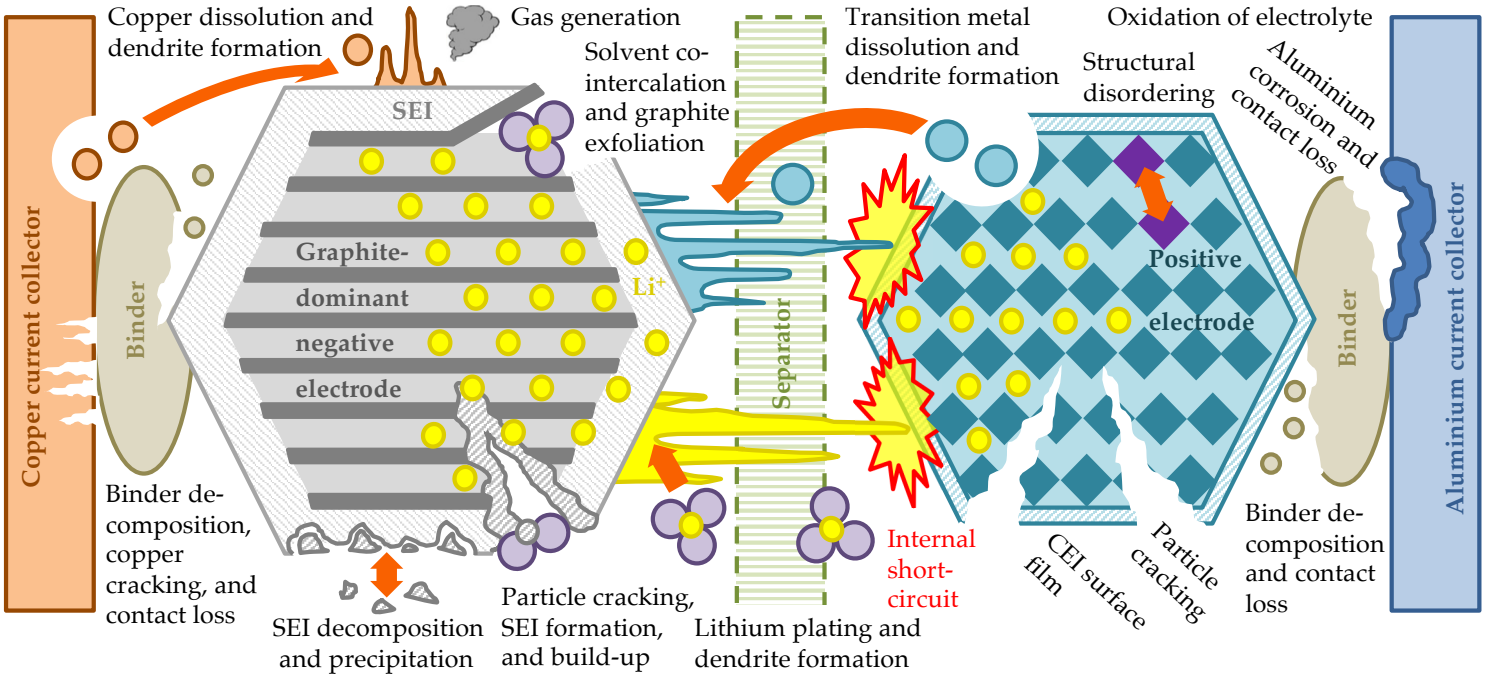

- Abundant literature describes these mechanisms qualitatively; an actively growing volume of research seeks to quantify the individual mechanisms and the interactions between them.
- We propose that, ideally, lithium-ion cells would last forever.
  - Lithium would cycle between electrodes without any loss in capacity and the dynamics governing a cell's voltage response to an input-current profile would not change over time.
- However, this is not what we observe in practice; instead, we notice *decreasing total capacity* and changes to cell dynamics—especially manifesting as *increases in cell resistance*—over time.
- These degradation indicators are: capacity fade and power fade.

Degradation modes

- Conceptually in-between low-level *degradation mechanisms* and high-level *degradation indicators* are degradation modes: loss of lithium inventory (LLI) and loss of active material (LAM).
- We illustrate how these two degradation modes lead to capacity fade.
- The figure shows ideal-cell behavior as a baseline: both electrodes have sixteen host sites; four and five negative- and positive-electrode sites are occupied.

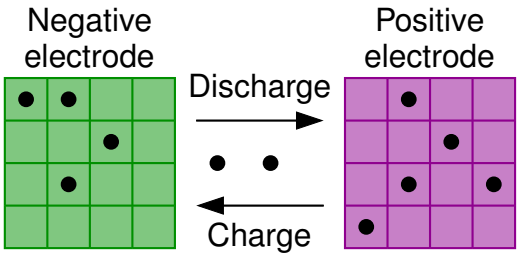

- When the cell is fully charged, there will be nine occupied sites in the negative electrode and no occupied sites in the positive electrode.
- When the cell is fully discharged, there will be no occupied sites in the negative electrode, and nine occupied sites in the positive electrode.
- Cell total capacity is the minimum of: number of negative-electrode sites, number of positive-electrode sites, and cyclable-lithium amount.
  - In this baseline case, total capacity $= \min\{16, 16, 9\} = 9$ Li atoms.
- Continuing the example, a side reaction is any undesired process that consumes lithium permanently so that it can no longer cycle.
- This degradation mode is known as loss of lithium inventory (LLI).
- The figure shows LLI where one lithium atom is consumed by a side reaction as the cell is being charged.

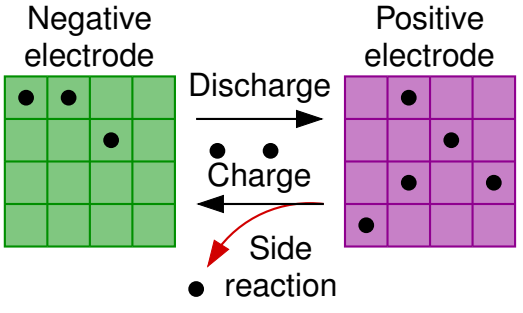

- Total capacity is reduced to the minimum of $\{16, 16, 8\} = 8$ Li atoms.

- Structural deterioration can also reduce capacity by eliminating lithium storage sites from one (or both) of the electrodes.
- This degradation mode is known as loss of active material (LAM), and is illustrated here as damage to the positive electrode (the white scar).

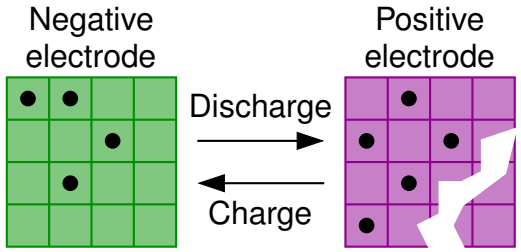

- Six sites in the positive electrode that previously could have held lithium are now unavailable to do so in the future.
  - Total capacity is now the minimum of $\{16, 10, 9\} = 9$ Li atoms.
  - Site loss did not alter total capacity even though damage occurred!
  - LAM can be invisible until its effect dominates other effects.
- If an electrode's structure deteriorates, lithium may become trapped.
  - Capacity is lost due to both LLI and LAM occurring simultaneously.
- In the figure, the lithium atom in the lower-right of the positive electrode is trapped by the structural collapse and is unavailable for cycling.

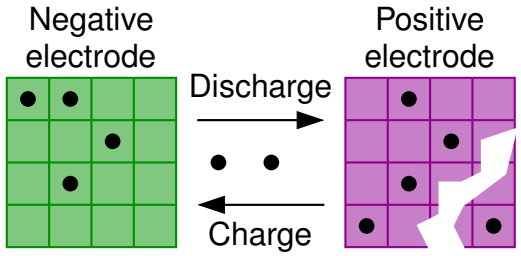

- The positive electrode now has ten useable storage sites.
  - Total capacity is the minimum of $\{16, 10, 8\} = 8$ Li atoms.

Capacity fade in terms of degradation modes

- In PBMs, cell total capacity can be expressed as:

$$Q = \underbrace{\frac{\varepsilon_s^n A L^n c_{s,\max}^n F}{3600}}_{Q^n} \underbrace{\left|\theta_{100}^n - \theta_0^n\right|}_{\Delta\theta_s^n} = \underbrace{\frac{\varepsilon_s^p A L^p c_{s,\max}^p F}{3600}}_{Q^p} \underbrace{\left|\theta_{100}^p - \theta_0^p\right|}_{\Delta\theta_s^p}.$$

- Until this point, we have treated all parameters as being constant.

- We now recognize that as a cell ages and capacity is lost, some of these parameter values must change.
  - We treat current-collector area A, electrode thickness L^{r}, and maximum lithiation $c^{\mathrm{r}}_{\mathrm{s,max}}$ as being constant to first order;
  - F and 3600 are physical constants and do not change;
  - So, capacity loss must be caused by changes to the solid volume fractions $\varepsilon^{\mathrm{r}}_{\mathrm{s}}$ and/or to electrode operating boundaries $\theta^{\mathrm{r}}_{100}$ and θ^{r}_{0}.
- LAM in one electrode directly decreases $\varepsilon^{\mathrm{r}}_{\mathrm{s}}$ for that electrode.
  - Therefore, we will see a decrease in Q^{r} for that electrode.
- However, LAM in one electrode does not cause LAM in the other; nevertheless, the equation for Q must still hold.
  - Therefore, if Q^{r} decreases in one electrode due to LAM, then $\Delta\theta^{\mathrm{r}}_{\mathrm{s}} = \left|\theta^{\mathrm{r}}_{100} - \theta^{\mathrm{r}}_{0}\right|$ must decrease in the other electrode.
- This is in fact what we observe, as we will explore in more detail later.
- It is less obvious from the equation how capacity is lost due to LLI.
  - Since the electrode materials are not themselves damaged by LLI, Q^{r} must remain constant for both electrodes.
  - So, $\left|\theta^{\mathrm{r}}_{100} - \theta^{\mathrm{r}}_{0}\right|$ must decrease in both electrodes. Again, we will see later that this is exactly what happens.
- Summarizing to this point:
  - Capacity loss is caused either by LLI or LAM (or both).
  - Can explain capacity loss by tracking changes to Q^{r}, $\theta^{\mathrm{r}}_{100}$, and θ^{r}_{0}.

Power fade in terms of degradation mechanisms

- While capacity fade can be categorized neatly in terms of LLI and/or LAM, it is less simple to categorize power fade.
- Anything that increases cell resistance is a cause of power fade; changes to nearly any parameter value in the cell model could do so.
- So it is worth reviewing the list of model parameters and considering which may change due to known degradation mechanisms.
- To be careful, we do so using standard parameters in case parameter lumping somehow obscures how aging changes some quantities.

Changes to $\varepsilon_{\mathrm{s}}^{\mathrm{r}}$: We begin by investigating what happens when $\varepsilon_{\mathrm{s}}^{\mathrm{r}}$ changes, as caused by any LAM mechanism. A decrease to $\varepsilon_{\mathrm{s}}^{\mathrm{r}}$:

- Decreases cell total capacity Q directly, as we have seen.
- Decreases conductivity $\bar{\sigma}^{\mathrm{r}} = \sigma_{\mathrm{eff}}^{\mathrm{r}} A / L^{\mathrm{r}}$ as $\sigma_{\mathrm{eff}}^{\mathrm{r}} = \sigma^{\mathrm{r}} (\varepsilon_{\mathrm{s}}^{\mathrm{r}})^{\mathrm{brug}}$ decreases.
- Increases film resistance $\bar{R}_{\mathrm{f}}^{\mathrm{r}} = R_{\mathrm{f}}^{\mathrm{r}} / (a_{\mathrm{s}}^{\mathrm{r}} A L^{\mathrm{r}})$ and double-layer resistance $\bar{R}_{\mathrm{dl}}^{\mathrm{r}} = R_{\mathrm{dl}}^{\mathrm{r}} / (a_{\mathrm{s}}^{\mathrm{r}} A L^{\mathrm{r}})$ since $a_{\mathrm{s}}^{\mathrm{r}} = 3\varepsilon_{\mathrm{s}}^{\mathrm{r}} / R_{\mathrm{s}}^{\mathrm{r}}$ decreases.
- Decreases rate constants $\bar{k}_{0,j}^{\mathrm{r}} = a_{\mathrm{s}}^{\mathrm{r}} A L^{\mathrm{r}} F k_{\mathrm{norm},0,\mathrm{j}}^{\mathrm{r}}$ since $a_{\mathrm{s}}^{\mathrm{r}}$ decreases.

- So, a decrease to $\varepsilon_{\mathrm{s}}^{\mathrm{r}}$ changes Q, $\bar{\sigma}^{\mathrm{r}}$, $\bar{R}_{\mathrm{f}}^{\mathrm{r}}$, $\bar{R}_{\mathrm{dl}}^{\mathrm{r}}$, $\bar{C}_{\mathrm{dl}}^{\mathrm{r}}$, $\bar{k}_{0,j}^{\mathrm{r}}$, and possibly $\bar{D}_{\mathrm{s}}^{\mathrm{r}}$.
- As already seen, it also changes θ_{100} and θ_0 in the opposite electrode.
- Most of these changes increase cell resistance.

Changes to $\varepsilon_{\mathrm{e}}^{\mathrm{r}}$: Certain kinds of degradation change porosity $\varepsilon_{\mathrm{e}}^{\mathrm{r}}$.

- For example, when solid–electrolyte interphase (SEI) film grows on the negative electrode, electrolyte solvent is consumed and volume previously occupied by electrolyte becomes filled with the SEI film.
- A decrease to $\varepsilon_{\mathrm{e}}^{\mathrm{r}}$:

- Decreases conductivity $\bar{\kappa}^{\mathrm{r}} = \kappa^{\mathrm{r}}_{\mathrm{eff}} A / L^{\mathrm{r}}$ as $\kappa^{\mathrm{r}}_{\mathrm{eff}} = \kappa^{\mathrm{r}} (\varepsilon^{\mathrm{r}}_{\mathrm{e}})^{\mathrm{brug}}$ decreases.
- Decreases the quantity of lithium in the electrolyte:

$$\bar{q}^{\mathrm{r}}_{\mathrm{e}} = \frac{\varepsilon^{\mathrm{r}}_{\mathrm{e}} c_{\mathrm{e},0} A L^{\mathrm{r}} F}{3600(1 - t^0_+)}.$$

- Decreases electrolyte diffusivity $\bar{D}^{\mathrm{r}}_{\mathrm{e}} = D^{\mathrm{r}}_{\mathrm{e,eff}} A c_{\mathrm{e},0} / (L^{\mathrm{r}}(1 - t^0_+))$ because $D^{\mathrm{r}}_{\mathrm{e,eff}} = D_{\mathrm{e}} (\varepsilon^{\mathrm{r}}_{\mathrm{e}})^{\mathrm{brug}}$ decreases.[1]

- So, decreasing $\varepsilon^{\mathrm{r}}_{\mathrm{e}}$ changes $\bar{\kappa}^{\mathrm{r}}$, $\bar{q}^{\mathrm{r}}_{\mathrm{e}}$, and $\bar{D}^{\mathrm{r}}_{\mathrm{e}}$; all increase resistance.

Other factors: Other degradation factors include:

- Binder decomposition (causing particle-to-particle contact loss),
- Delamination of the electrode from the current collector (which causes particle-to-current-collector contact loss) and
- Current-collector corrosion, all of which decrease the conductivity of the electrode taken as a whole (effectively reducing A) and increase contact resistance R_{c}.

- There are even some degradation mechanisms that can lead to a short-term *decrease* in cell resistance.
  - For example, electrode swelling and shrinking caused by repeated de/intercalation can crack the SEI film, making it locally easier for de/intercalation, thus reducing $\bar{R}^{\mathrm{n}}_{\mathrm{f}}$.
  - However, cracks in the SEI expose fresh graphite to the electrolyte and SEI film quickly regrows, restoring the prior level of resistance.
- In summary, any aging mechanism that leads to a decrease in either $\varepsilon^{\mathrm{r}}_{\mathrm{s}}$ or $\varepsilon^{\mathrm{r}}_{\mathrm{e}}$ will tend to increase cell resistance indirectly.
- Some mechanisms operate directly on specific terms in the model such as $\bar{R}^{\mathrm{r}}_{\mathrm{f}}$, increasing resistance in a more straightforward ways.

[1] $\bar{D}^{\mathrm{r}}_{\mathrm{e}}$ is not part of the LPM: changes to its value are observable only via $\bar{\psi} = F \bar{D}^{\mathrm{r}}_{\mathrm{e}} / (T \bar{\kappa}^{\mathrm{r}})$.

6.3: Diagnosis versus prognosis

- How should a BMS respond to cell aging over the pack's life?
- First, we recognize that BMS state estimates and control decisions are likely to degrade if the BMS does not account for cell aging.
  - We expect improved estimates if the BMS always has models of every pack cell that accurately describes their present dynamics.
- So, the first important BMS response to aging is diagnostics.
  - We use this term to refer to methods that provide up-to-date aged-cell parameterized models of every cell in a battery pack.[2,3]
  - We use the term almost in a medical sense, to determining what is going wrong with a cell even (and especially) if it has not yet failed.
  - We are not interested in postmortem diagnostics of failed cells, but rather in diagnostics that apply to aged but still-useable cells.
- Second, we recognize that control actions a BMS should take with an aged cell are likely to be different from those that apply to a fresh cell.
  - We must account for the present aging state to minimize near-term degradation predicted to be caused by any proposed action. Then,
  - Optimize actions to minimize anticipated incremental degradation.
- So, the second BMS response to aging involves prognostics.
  - We use this term to refer to a cell's predicted near-future condition if some proposed current or power profile were to be applied to it.[4]

[2] This is an advanced proxy to simpler state-of-health estimation.

[3] This definition is broader than one often used in prognostics and health management (PHM) literature, which more narrowly to relate to detecting faults and failures.

[4] Again, this definition is broader than is commonly encountered in the PHM literature, which focuses on remaining useful life (RUL) of components or systems.

  - Here, we are less concerned with predicting RUL (or the point in time of complete failure of the battery pack) than with predicting quantities such as the amount of short-term future degradation.

- In summary, we refer to diagnostics as methods to determine the present SOH as specifically as possible.
  - We would like to find model parameter values that accurately describe every cell's dynamics at its present state of aging.
  - These diagnostics include updating a total-capacity estimate as is common with SOH estimators, but also ideally updating many or all of the remaining LPM parameter values as well.
- We refer to prognostics as predictive of the future condition of the cell, including how some or all of the LPM parameters are expected to change if some user-provided current or power profile were applied.
  - These predictions can be used in optimizations within fast-charge and dynamic-power-limit algorithms, for example.
- If we are able to perform diagnostics well, we can assume that BMS state estimates will be good.
- If we are able to perform short-term prognosis well, we can assume that BMS optimized control decisions will be good.
- In the next sections, we provide a survey of some diagnostics and prognostics methods. But, before we do so, we pose two questions:
- **Re. diagnostics**: How important is it for a BMS to have accurate aged-cell models of all of its cells vs. a single fresh-cell model?
  - Maybe not as much as we might expect, especially if we use an adaptive model-based state-estimation method (e.g., SPKF).

- The adaptivity of the SPKF can overcome much of the anticipated state-prediction errors due to voltage-prediction errors caused by mismatch between the BOL embedded model versus present cell dynamics when computing state estimates.
- This result is encouraging because it implies that our diagnostics need neither be comprehensive nor perfect for the identified aged-cell models to be useful.

- **Re. prognostics**: How important is it for a BMS to compute RUL?
  - There is perhaps more current debate on this topic.
  - I agree that it is important for some applications—such as:
    - Sizing a battery when designing a battery pack—to be able to predict RUL in simulation studies under anticipated usage.
    - Determining whether a battery pack is suitable for use in a second-life application.
    - Fleet operators need to be able to plan ahead.
  - But, my present opinion is that it is not necessary for a real-time BMS in most applications to be able to predict far-future RUL.
  - It may be valuable to notify battery operators that failure is likely in the next minutes or days so that they can take any necessary actions to protect themselves and ancillary equipment.
  - But, I feel that it is of little use to make real-time statements such as “the battery is expected to have an RUL of 8.75 years,” given the uncertainties in making far-future predictions.
  - Exception: Fleet operators must be able to plan purchases; still, the RUL estimates are not needed in real time.

6.4: Changes to OCV, θ_0^{r}, and $\theta_{100}^{\mathrm{r}}$ as a diagnostic

- Different levels of diagnostics information exist that might be helpful.
  - Capacity and power fade can be diagnosed using standard SOH methods that estimate total capacity Q and series resistance R_0.
  - But it could be helpful if we could discern the causes of capacity and power fade, perhaps by quantifying the levels of LLI or LAM, or even in estimating changes to other model parameter values.
- One of the simplest reported advanced diagnostics monitors changes to the cell's OCV vs. SOC relationship and the corresponding shifts in the electrode stoichiometric operating windows.
  - For now, we assume that we have lab-quality OCV relationships that we can use, but will consider real-time application later.

Changes to OCV due to LLI

- When studying the effects of LLI and LAM, recall:

$$Q = \frac{\varepsilon_{\mathrm{s}}^{\mathrm{r}} A L^{\mathrm{r}} c_{\mathrm{s,max}}^{\mathrm{r}} F}{3600} \left| \theta_{100}^{\mathrm{r}} - \theta_0^{\mathrm{r}} \right| = Q^{\mathrm{r}} \Delta\theta_{\mathrm{s}}^{\mathrm{r}}.$$

- Under LLI, neither of the electrode absolute capacities Q^{r} change.
- So, reduction in Q must come from a decrease $\Delta\theta_{\mathrm{s}}^{\mathrm{r}}$ in both electrodes.
- We illustrate this mathematical reality with a thought experiment.
  - Let us assume that a cell is initially resting at 100 % SOC prior to losing lithium in the negative electrode. At this point, $\theta_{\mathrm{s}}^{\mathrm{r}} = \theta_{100}^{\mathrm{r}}$.
  - This is illustrated the figures by the blue markers.
- LLI in the negative electrode decreases $\theta_{\mathrm{s}}^{\mathrm{n}}$ as lithium is extracted from the electrode to take part in side reactions (cf. the red marker).

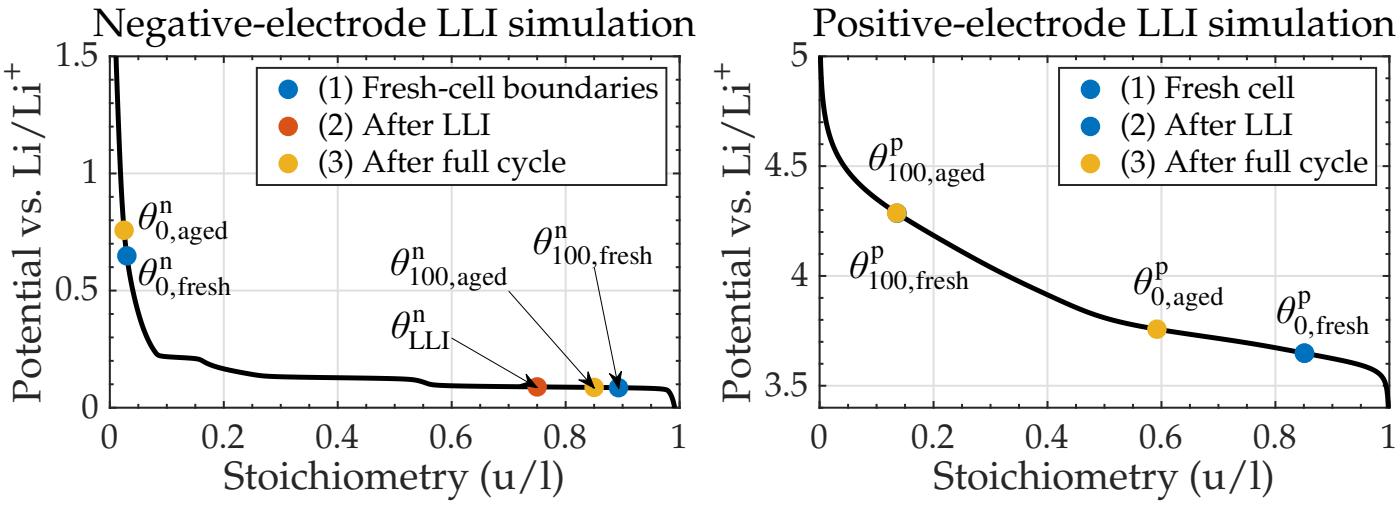

- Since θ_s^p does not change, $U_{ocp}^n(\theta_s^n)$ increases while $U_{ocp}^p(\theta_s^p)$ remains constant. Overall, cell voltage decreases.
- We will not notice the impact of LLI on electrode operating boundaries until we perform a full charge and discharge of the cell.
- Since LLI has decreased cell voltage, we must add charge to the cell to return OCV to v_{max}, which is our definition for 100 % SOC.
- Adding charge decreases θ_s^p, which was already at its prior lower limit of θ_{100}^p. So, θ_{100}^p moves left and $U_{ocp}^p(\theta_{100}^p)$ increases vs. its prior value.
- Since $U_{ocp}^p(\theta_{100}^p)$ increases, $U_{ocp}^n(\theta_{100}^n)$ must also increase for the OCV to equal v_{max}, meaning that θ_{100}^n is less than before aging due to LLI.
- When we discharge to v_{min} (conserving Li), θ_0^r in both electrodes decrease vs. prior values. All boundaries decrease, but the dominant effect is that the window width $\Delta\theta_s^r$ shrinks in both electrodes.
- LLI at other conditions has an identical effect.
- The figures below show simulation-study results exploring electrode operating-boundary movement due to LLI for a graphite//NMC cell.
  - Arrows indicate directions that the boundaries move.

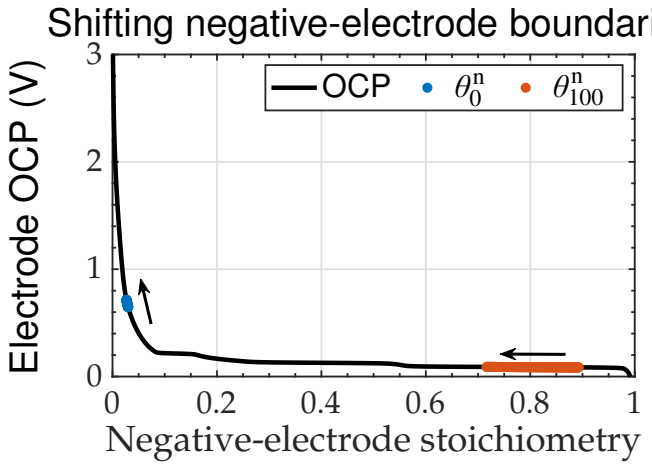

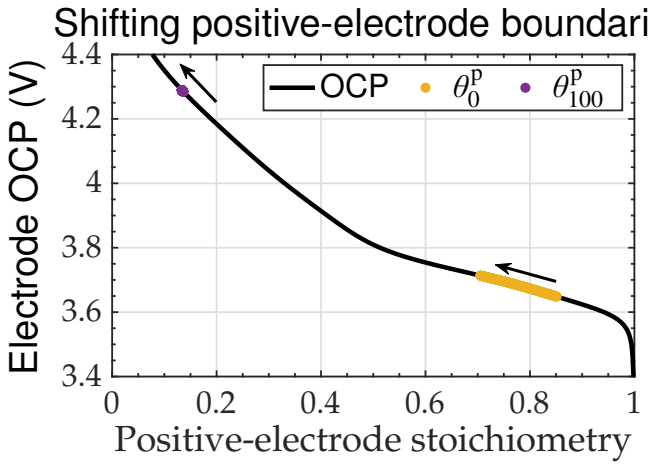

- LLI in the negative and positive electrodes and at several different initial SOC points were explored. The results from the different scenarios are visually (and perhaps actually) indistinguishable.
- The next figures show the evolution of OCV and differential OCV.

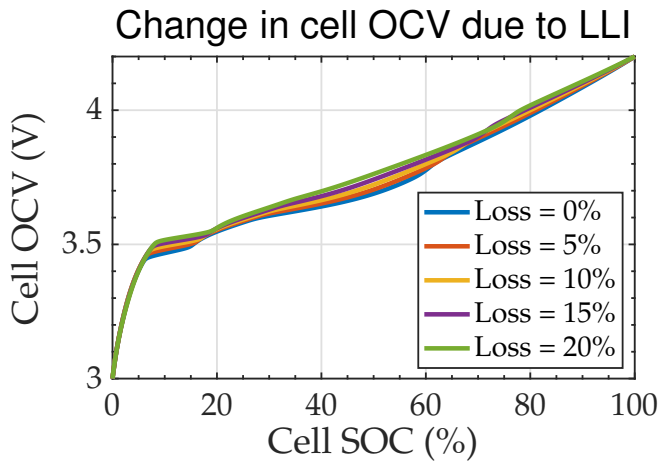

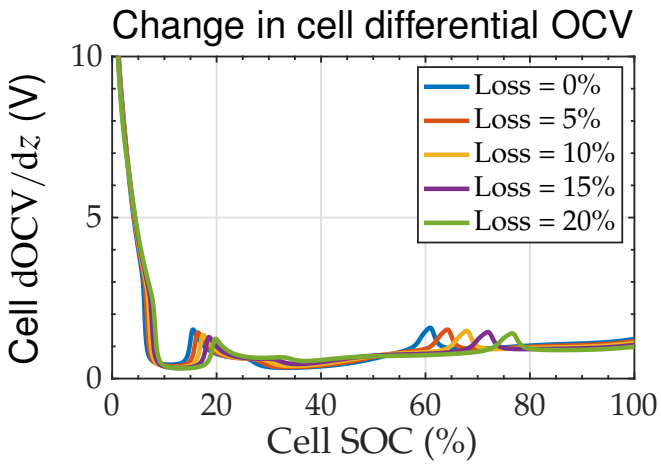

- When all aging is due to LLI, we see noticeable changes to OCV and differential OCV that might help diagnose the level of cell degradation.

Changes to OCV due to LAM

- Changes to OCV due to LLI do not appear to depend on the electrode in which the lithium is lost or the cell SOC at which the loss occurs.
- LAM operates differently. To illustrate, we consider two scenarios.

SCENARIO I: Some small amount of nonlithiated active material is lost (in the negative) when the cell is initially resting at 100 % SOC.

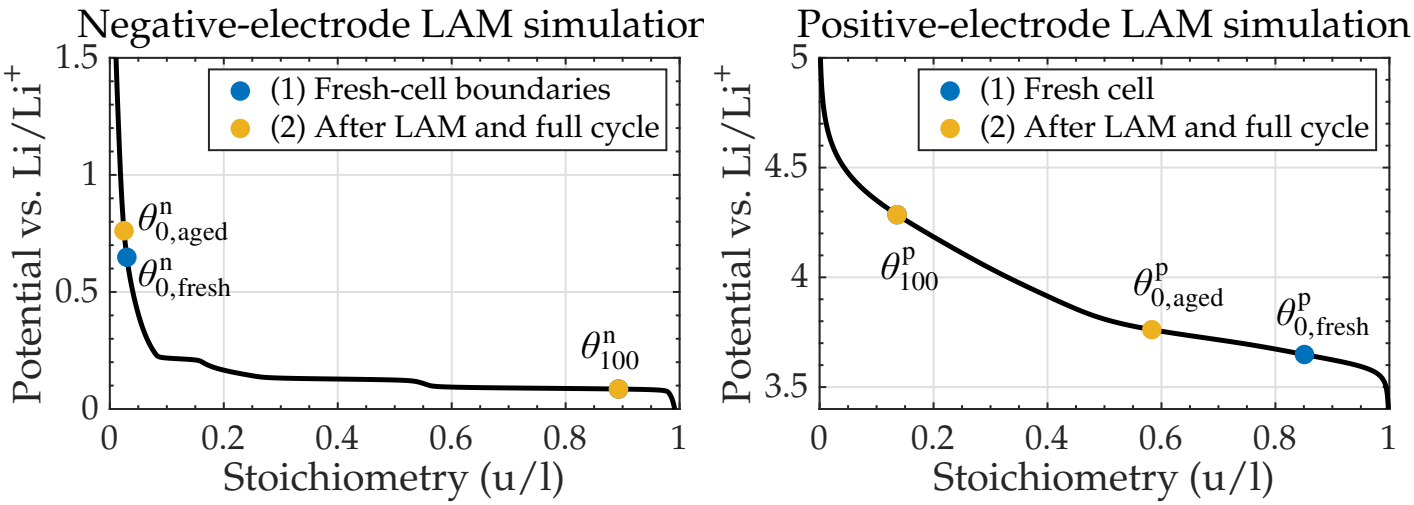

- Since no lithium inventory is lost, cell voltage does not change. So, the cell remains at 100 % SOC and neither $\theta^{\mathrm{n}}_{100}$ nor $\theta^{\mathrm{p}}_{100}$ change.
- But, since $\varepsilon^{\mathrm{r}}_{\mathrm{s}}$ decreases, capacity Q^{r} for that electrode decreases.
- To balance the operational capacities of both electrodes, $\Delta\theta^{\bar{\mathrm{r}}}_{\mathrm{s}}$ for the opposite electrode $\bar{\mathrm{r}}$ must decrease, shrinking the OCP range of $\bar{\mathrm{r}}$.
- To maintain cell voltage limits of $v_{\min}$ and $v_{\max}$, $\Delta\theta^{\mathrm{r}}_{\mathrm{s}}$ must increase for the region that loses the active material.
- This is illustrated above for the case when LAM occurs in the negative electrode when the cell is initially resting at 100 % SOC.

SCENARIO II: Active material is lost (in positive) when cell SOC is 0 %.

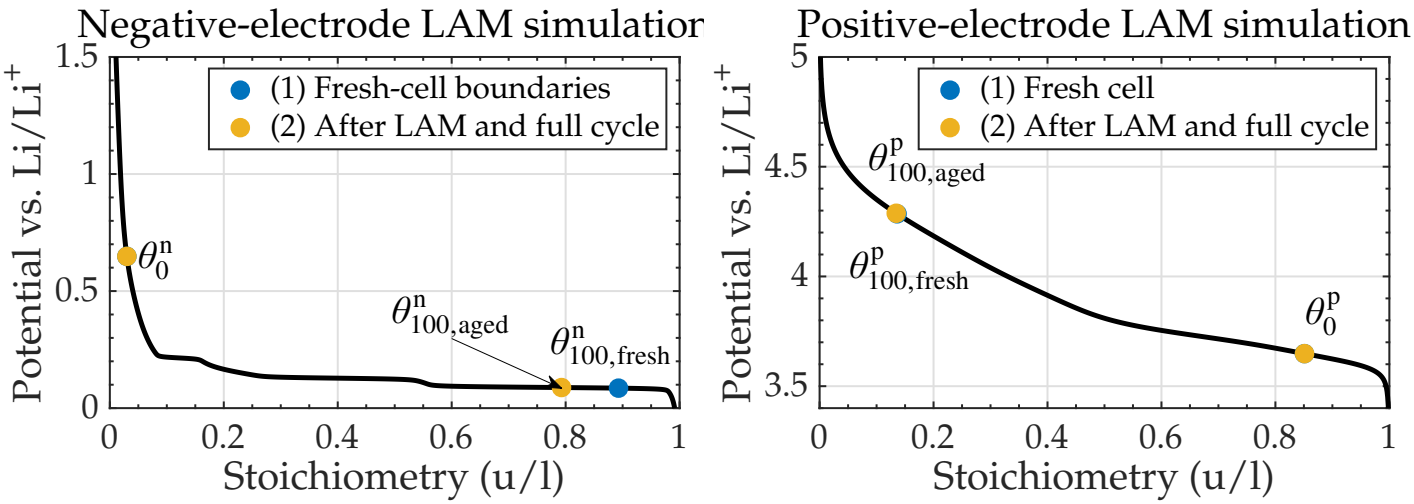

- We again consider losing nonlithiated material, so there is no loss of lithium inventory. As no lithium is lost, cell voltage does not change.
- Therefore, the cell remains at 0 % SOC and neither θ_0^{n} nor θ_0^{p} change.
- However, since $\varepsilon_{\mathrm{s}}^{\mathrm{r}}$ decreases, the Q^{r} for that electrode decreases.
- To balance the operational capacities of both electrodes, $\Delta\theta_{\mathrm{s}}^{\bar{\mathrm{r}}}$ for $\bar{\mathrm{r}}$ must decrease, forcing the OCP range of $\bar{\mathrm{r}}$ to shrink.
- In order to maintain cell voltage limits $v_{\min}$ and $v_{\max}$, the value of $\Delta\theta_{\mathrm{s}}^{\mathrm{r}}$ must increase for the region that loses the active material.
- This is illustrated above for the case when LAM occurs in the positive electrode when the cell is initially resting at 0 % SOC.
- Summary: $\theta_{\mathrm{s}}^{\mathrm{r}}$ doesn't change for SOC at which material is lost, $\Delta\theta_{\mathrm{s}}^{\mathrm{r}}$ increases for electrode that loses material and decreases for other.
  - Material lost at 0 % SOC: θ_0^{r} don't change but both $\theta_{100}^{\mathrm{r}}$ change;
  - Material lost at 100 % SOC: $\theta_{100}^{\mathrm{r}}$ don't change but both θ_0^{r} change;
  - When active material is lost at other SOCs, all boundaries change.
- Figures below show simulation results when active material is lost in the negative electrode when the cell is initially resting at 100 % SOC.

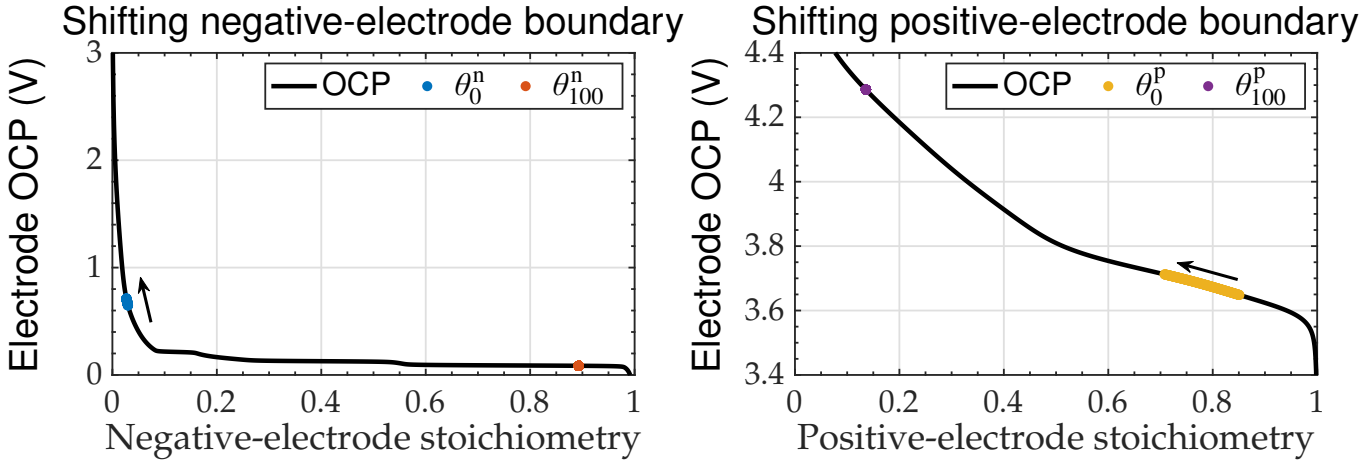

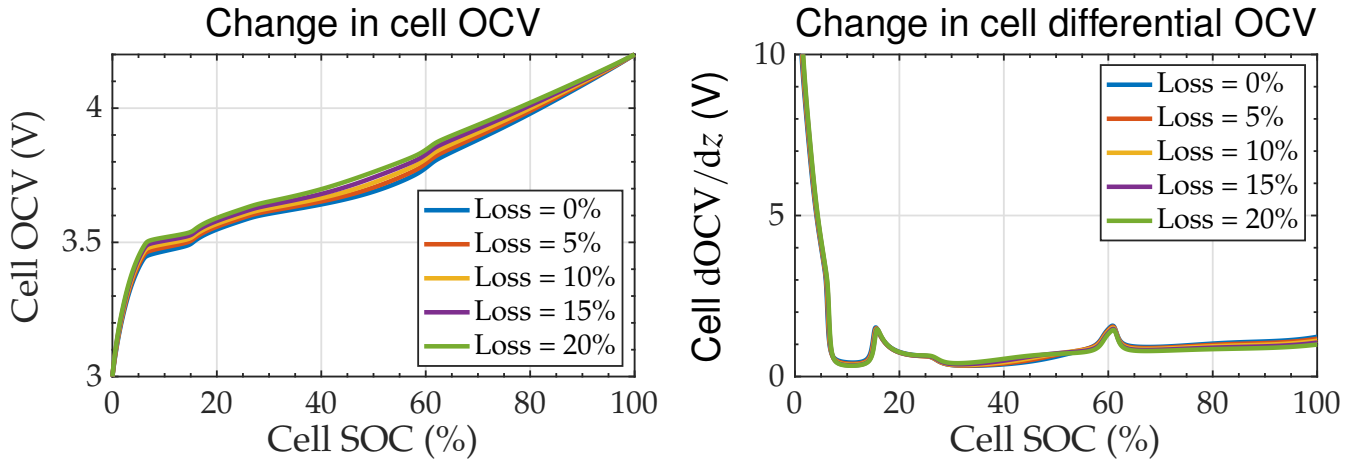

- The figures below show simulation results when active material is lost in the positive electrode when the cell is initially resting at 0 % SOC.

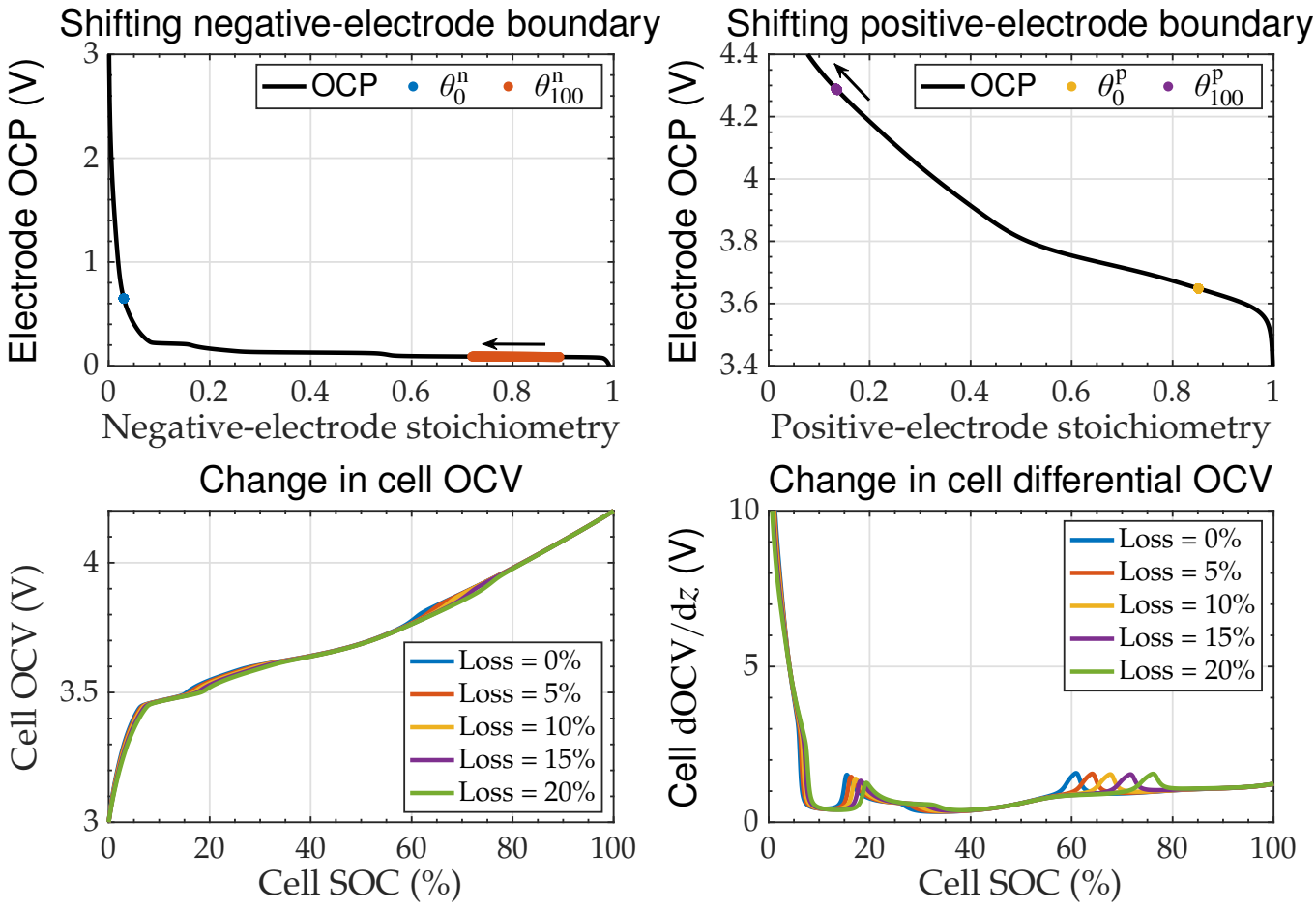

- The simulation results confirm our discussion regarding how the operating boundaries are expected to move, and provide further insight into the changes to cell OCV and differential OCV.

- Unlike the LLI case, each LAM scenario changes OCV differently.
- But, assuming that electrode OCP relationships themselves do not change as a cell ages, we can fit electrode operating boundaries θ_0^{r} and $\theta_{100}^{\mathrm{r}}$ to match electrode OCP relationships to the aged-cell OCV to determine how the stoichiometric windows change due to age.
- We may also be able to determine how much LLI and LAM have occurred, and in which electrodes.
- But, to do so requires an accurate estimate of the present cell OCV relationship, which requires lab equipment and specialized testing.
- In the next section, we review a method that may be able to accomplish similar objectives in a practical BMS in real time.

6.5: Loosely coupled tracking of θ_s^r in both electrodes

- We now recognize that the stoichiometric operating windows of both electrodes change as a cell ages.
  - Using lab-quality OCV data, we can estimate θ_0^r and θ_{100}^r;
  - However, this is not feasible for a real-time BMS application.
- Allam and Onori have proposed a real-time architecture to estimate θ_s^r reliably in both electrodes.
- They use separate models of negative- and positive-electrode dynamics that are loosely coupled.
- Each model employs a closed-loop estimator of the state dynamics for the electrode it describes directly, and an open-loop predictor of the dynamics of the opposite electrode.
- The models are interconnected by providing the closed-loop estimate from one as the input to the open-loop predictor of the other.

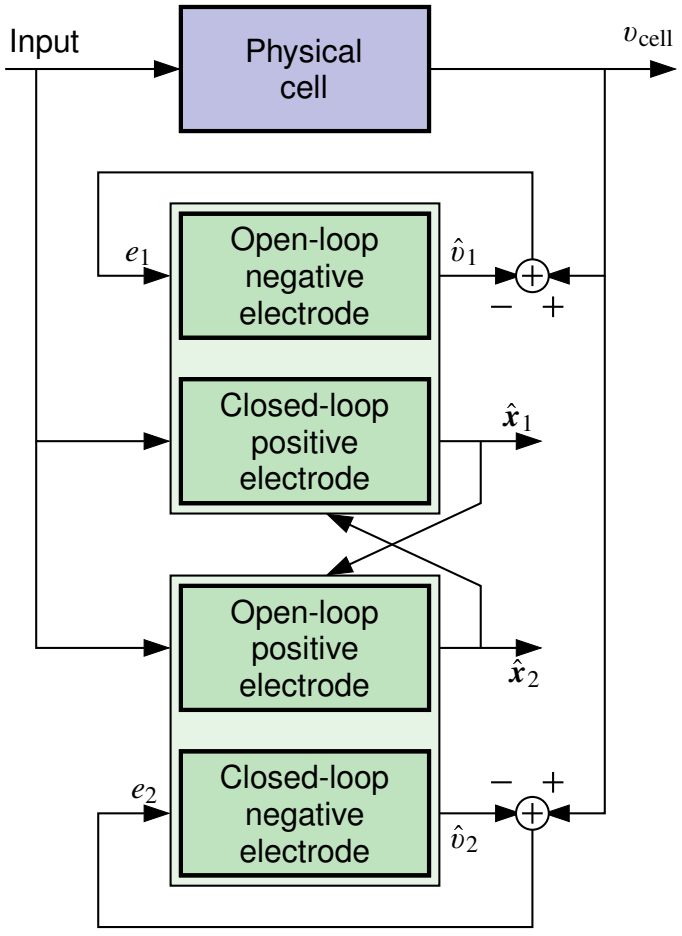

- By adapting the state estimate of both electrodes separately, they adjust somewhat independently of one another and track θ_s^r correctly for both electrodes, even when the operating windows change.
- To be more specific, the positive-electrode model is defined in a continuous-time state-space form as:

$$\dot{\hat{\boldsymbol{x}}}_1(t) = \boldsymbol{A}_{11}\hat{\boldsymbol{x}}_1(t) + \boldsymbol{B}_1 u(t) + \mathbf{fn}_1(v_{\text{cell}}(t) - \hat{v}_1(t))$$

$$\dot{\hat{\boldsymbol{x}}}_{2,\text{ol}}(t) = \boldsymbol{A}_{22}\hat{\boldsymbol{x}}_2(t) + \boldsymbol{B}_2 u(t)$$

$$\hat{v}_1(t) = h_1(\hat{\boldsymbol{x}}_1(t), u(t)) - h_2(\hat{\boldsymbol{x}}_{2,\text{ol}}(t), u(t)) - R_0 u(t),$$

where $\boldsymbol{x}_1(t)$ is the state of the positive-electrode model, $\boldsymbol{x}_2(t)$ is the state of the negative-electrode model, $u(t)$ is the input current, $v_{\text{cell}}(t)$ is the actual cell voltage, and $\hat{v}_1(t)$ is the prediction of cell voltage computed by this model.

- The matrices $\boldsymbol{A}_{11}$, $\boldsymbol{A}_{22}$, $\boldsymbol{B}_1$, and $\boldsymbol{B}_2$ are provided by the models of the two electrodes.
- The function $\mathbf{fn}_1(\cdot)$ is a possibly nonlinear feedback calculation.
- The function $h_1(\cdot)$ computes the positive-electrode OCP and Butler–Volmer overpotential; the function $h_2(\cdot)$ computes the negative-electrode OCP and Butler–Volmer overpotential.

- This model adjusts the positive-electrode state estimate using a feedback mechanism and computes an open-loop prediction of the negative-electrode state using the most recently available closed-loop estimate from the opposite observer.
- It predicts cell voltage (lumping all electrolyte dynamics into the Ohmic resistance term R_0) and uses the voltage-prediction error to adapt its own state estimate.
- The negative-electrode model computes a symmetric relationship:

$$\dot{\hat{\boldsymbol{x}}}_{1,\text{ol}}(t) = \boldsymbol{A}_{11}\hat{\boldsymbol{x}}_1(t) + \boldsymbol{B}_1 u(t)$$

$$\dot{\hat{\boldsymbol{x}}}_2(t) = \boldsymbol{A}_{22}\hat{\boldsymbol{x}}_2(t) + \boldsymbol{B}_2 u(t) + \mathbf{fn}_2(v_{\text{cell}}(t) - \hat{v}_2(t))$$

$$\hat{v}_2(t) = h_1(\hat{\boldsymbol{x}}_{1,\text{ol}}(t), u(t)) - h_2(\hat{\boldsymbol{x}}_2(t), u(t)) - R_0 u(t).$$

- Here, the positive-electrode state evolves open-loop and the negative-electrode state evolves according to a feedback law.
- Allam and Onori used an SPM and sliding-mode observers.
  - A more recent paper uses three interconnected SPKFs with an SPMe model to estimate electrode and electrolyte state;[5]
  - A companion work shows how to use a similar mechanism also to estimate θ_0^{r}, $\theta_{100}^{\mathrm{r}}$, and $\varepsilon_{\mathrm{s}}^{\mathrm{r}}$.[6]

[5] I. Lopetegi, G.L. Plett, M.S. Trimboli, A.K. de Souza, L. Oca, E. Miguel, U. Iraola, "A new battery SOC/SOH/eSOH estimation method using a PBM and interconnected SPKFs: Part 1. SOC and internal variable estimation," *J. Electrochem. Soc.*, 171(3), 2024, 030519.

[6] I. Lopetegi, G.L. Plett, M.S. Trimboli, L. Oca, E. Miguel, U. Iraola, "A new battery SOC/SOH/eSOH estimation method using a PBM and interconnected SPKFs: Part 2. SOH and eSOH estimation," *J. Electrochem. Soc.*, 171(3), 2024, 030518.

6.6: Adapting a model to track cell variations and aging

- The Allam and Onori method uses a fixed fresh-cell model to estimate individual electrode stoichiometries.
- We expect that if more model parameter values could be adjusted reliably, better estimates could be made.
- One approach is to adapt model parameter values so that the model's predictions match the physical cell's input/output (current/voltage) behaviors.

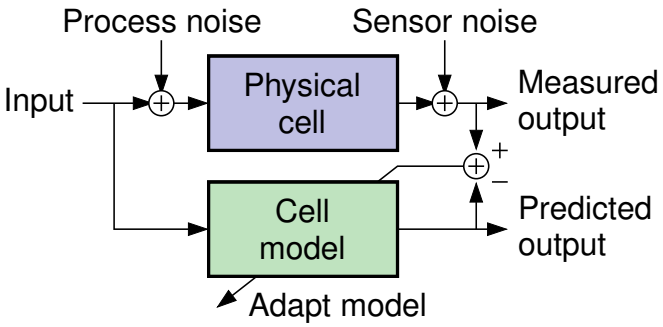

- A clever approach combines a fixed fresh-cell physical model with machine-learning (ML, e.g., a neural network (NN)).
- All dynamic effects are captured by the physical model; the NN simply computes a static nonlinear function of its inputs to improve model predictions.

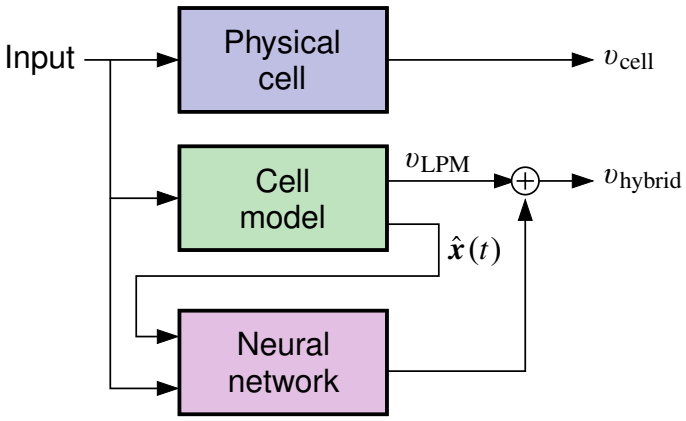

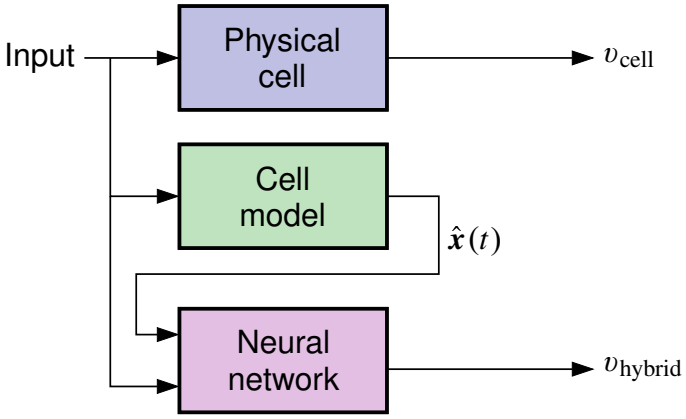

- In the top figure, the physical cell model produces a voltage estimate $v_{\text{LPM}}(t)$ and its own internal state estimate $\hat{\boldsymbol{x}}(t)$.
- The NN computes a correction factor based on $i_{\text{app}}(t)$ and $\hat{\boldsymbol{x}}(t)$.
- The correction factor is added to $v_{\text{LPM}}(t)$ to produce the overall hybrid voltage prediction, $v_{\text{hybrid}}(t)$.

- The NN parameters are adapted using standard ML methods such that $v_{\text{hybrid}}(t)$ agrees with $v_{\text{cell}}(t)$ as closely as possible.
- In the bottom figure, the physical cell model simply produces its own internal state estimate and the NN directly computes $v_{\text{hybrid}}(t)$ based on $\hat{\boldsymbol{x}}(t)$ and $i_{\text{app}}(t)$.
- While adaptation is appealing in principle, it is risky.
  - It is inherently difficult to separate the influence of the slowly aging parameters from the rapidly moving state.
  - Even more difficult if parameters and outputs are loosely related.
  - It is very difficult to "tune" generic adaptive methods to adjust parameters to physically meaningful values instead of simply matching short-term input/output observations.
- Adjusting parameters using long data records can help; modifying only a subset of parameters can also lead to more stable behaviors.
- The hybrid ML methods on the prior page promise to be more stable than if we were to adjust the state and parameters of the physical model directly.
- The big advantage is that all dynamics are in the fixed physical model.
- The physical model does not adapt in this scenario, and so state updates will not lose physical meaning.
- The neural-network component simply acts to improve the estimates by providing a static (i.e., memoryless) nonlinear correction factor that can adapt to model the cell at different states of age.

6.7: Tracking cell variations and aging via selective approaches

- In contrast to the adaptive avenue, a second approach is to select from a database of pre-aged models the one that best describes observed dynamics.

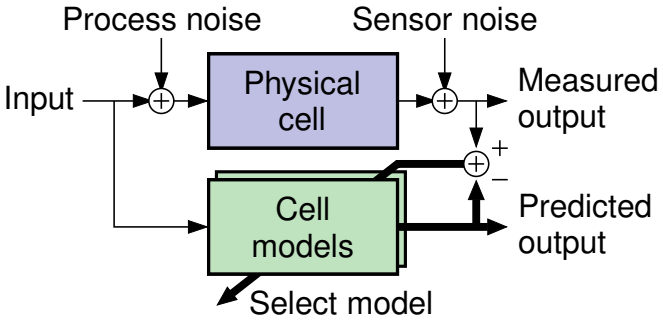

- Unlike the parameter-adaptation method, the database of preaged models used by this approach can be constrained to guarantee physically realistic parameter sets.
- However, more computation and storage are needed vs. adaptation.
- This model-selection approach can be implemented using interacting multiple model Kalman filters (IMM-KF).
- One fresh-cell model is combined with multiple aged-cell models.

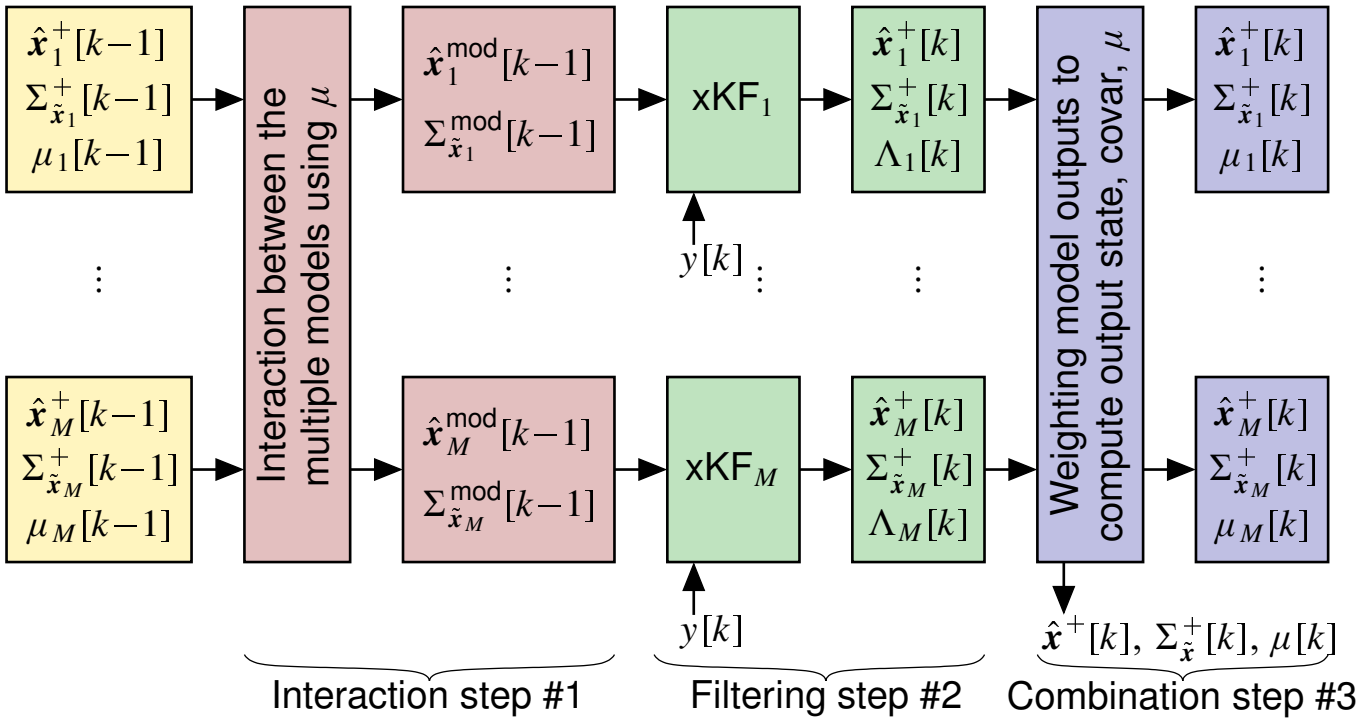

- The IMM executes one KF per model, in parallel, and blends KF state estimates based on match between model and observed dynamics.
- It also produces a pmf indicating the likelihood of any of the models being the one that best describes the cell at its present state of age.
- In the IMM block diagram, each of the M rows represents a Kalman filter, one per model in the model set.
- Each iteration, the inputs are the prior state and covariance estimates for each model, as well as a pmf $\boldsymbol{\mu}_j$, which estimates the probability that the cell was best described by the jth model at the prior timestep.
- The IMM first performs an interaction step, which combines these estimates based on a transition-probability matrix $\boldsymbol{p}_{ij}$ that describes the likelihood of moving from model i to model j between timesteps.
- Then, individual KFs update state estimates, error covariances, and likelihoods of the measured voltage given the assumed models.
- The combination step weights KF outputs to compute an overall state estimate, covariance, and pmf.

- To apply the IMM to the BMS model-selection problem, we must first develop models that are representative of a cell at different states of age.
- The figure shows an example matrix of models comprising a single fresh-cell model and 20 additional aged-cell models.

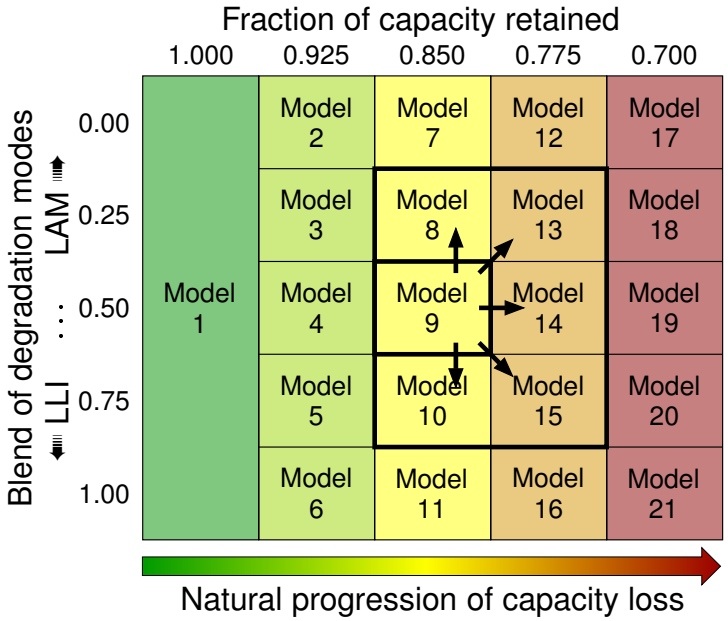

- The aged models represent a hypothetical cell at levels of retained capacity equal to 92.5 %, 85 %, 77.5 %, and 70 % of original capacity.
- They also represent cells having degraded entirely due to LLI or entirely due to LAM or due to some blend of the two.
- In addition to the aged models, we must provide a model-transition matrix $\boldsymbol{p}$ containing the probability of transitioning from model i to model j:

$$\boldsymbol{p}_{ij} = \Pr\left(m[k] = j \mid m[k-1] = i\right),$$

  where $m[k]$ is the model that best describes the cell at time k.
- The above figure shows the assumption made by Smiley and Plett, that a cell cannot regain lost capacity, and so the transitions are never toward the left in the model space.
- Generally, the values on the diagonal of $\boldsymbol{p}_{ij}$ are very close to 1, indicating that it is most likely that the model that describes a cell does not change from one timestep to another.
- Models that are adjacent to the present model have small positive values in $\boldsymbol{p}_{ij}$; models that are not adjacent have zeros values in $\boldsymbol{p}_{ij}$.
- Figure to right shows evolution of $\boldsymbol{\mu}_j$ versus time in the IMM.
- We might consider using this pmf to select the model from the model space that best describes the input/output observations.
- Here, the j that maximizes $\boldsymbol{\mu}_j$ correctly identifies the true model.

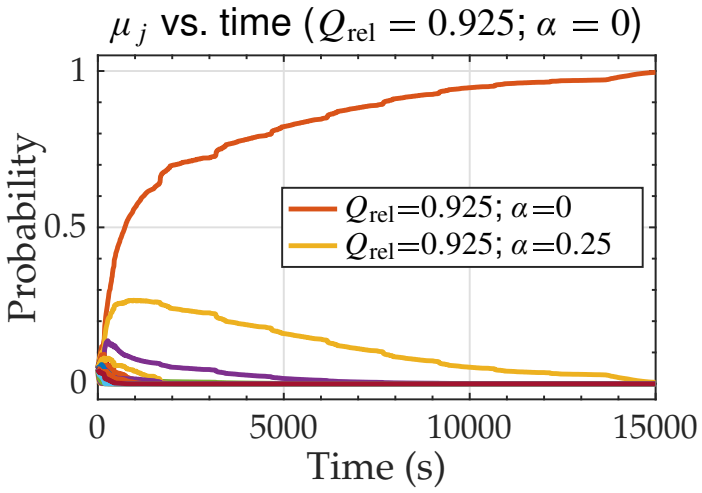

- In the top plot, the j that maximizes μ_j again correctly identifies the true model.
- In the lower plot, it instead identifies a nearest-neighbor model having nearly identical input/output dynamics.
- Only toward the very end of the simulation does the IMM appear to recognize its error and begin to correct the values of μ_j.
- The nearest-neighbor model incorrectly selected at first is likely to be sufficient for BMS application

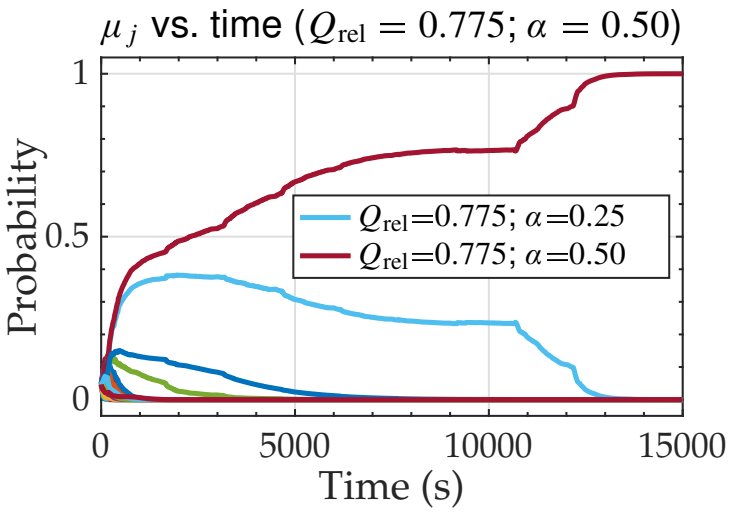

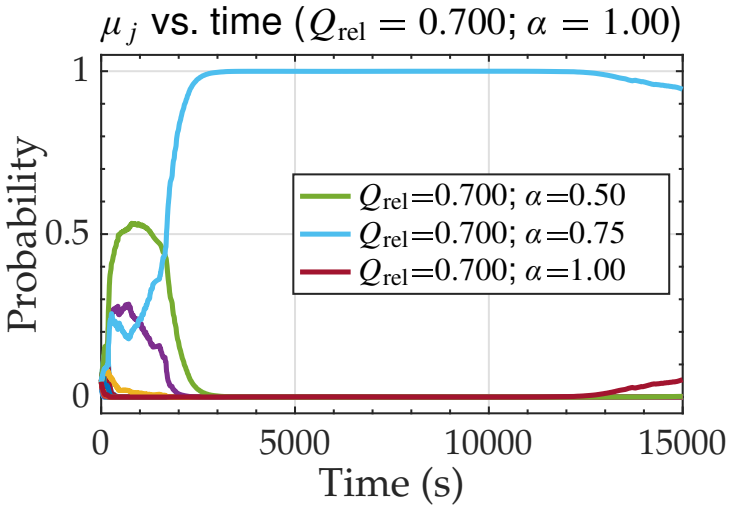

- While model selection using an IMM can work well, it is a computationally intensive approach.
- We find that it tends to work best when the cell voltage dynamics are very different from one model to another, which isn't always the case.
- State estimates are always good but the correct model is not always selected from the model set; as we have seen, it sometimes selects a nearest-neighbor model having similar dynamics.
- More work could be done to optimize the model-set design to maximize distance between nearest neighbors in a dynamic sense.

6.8: BMS prognostics and cell 1D thermal model

- Now that we have quickly surveyed some BMS diagnostics topics, we turn our attention to prognostics.
  - Broadly, prognostics involve predicting a future cell condition.
- In this chapter, we introduce a 1D lumped-parameter thermal model and a degradation model as prognostics.
  - These will be used later when implementing BMS controls.

Cell 1D thermal model

- This section considers adding a description of heat generation and temperature evolution to the cell model.
- Cell dynamics and degradation mechanisms are highly temperature-dependent; thus, predicting temperature is important BMS task.
- A thermal model can predict cell core temperatures and act as virtual temperature sensors for cells that are not monitored directly.
- BMS can measure cell surface temperature, but to predict the future thermal effect of a proposed control action, we need a thermal model.
  - In that sense, a thermal model provides prognostic information.

Converting thermal model into lumped-parameter form

- Here, we convert the physics-based 1D DFN-style model from ECE5710 to use inputs from the LPM. As a reminder, the model was:[7]

$$\frac{\partial(\rho^{\mathrm{r}} c_{\mathrm{P}}^{\mathrm{r}} T^{\mathrm{r}})}{\partial t} = \nabla \cdot (\lambda^{\mathrm{r}} \nabla T^{\mathrm{r}}) + q^{\mathrm{r}}, \tag{6.1}$$

[7] We omit discussion of the PDE's boundary conditions here; we assume convective heat transfer at the cell surface, but this could be extended as described in ECE5710.

where ρ^{r} is the material density of cell region r, $c_{\mathrm{P}}^{\mathrm{r}}$ is the specific heat, $T^{\mathrm{r}}(x,t)$ is the temperature in kelvin, λ^{r} is the thermal conductivity, and q^{r} is the heat-generation rate in $\mathrm{W\,m^{-3}}$.

- The heat-generation term itself summed different heat sources:

$$q^{\mathrm{r}} = q_{\mathrm{i}}^{\mathrm{r}} + q_{\mathrm{r}}^{\mathrm{r}} + q_{\mathrm{e}}^{\mathrm{r}} + q_{\mathrm{s}}^{\mathrm{r}} + q_{\mathrm{c}}^{\mathrm{r}},$$

  - Irreversible heat generation due to reactions: $q_{\mathrm{i}}^{\mathrm{r}} = a_{\mathrm{s}}^{\mathrm{r}} F j_j^{\mathrm{r}} \eta_j^{\mathrm{r}}$ for each chemical reaction j that takes place at solid/electrolyte interface;
  - Reversible heat gen. due to entropy change: $q_{\mathrm{r}}^{\mathrm{r}} = a_{\mathrm{s}}^{\mathrm{r}} F j_j^{\mathrm{r}} T \dfrac{\partial U_{\mathrm{ocp},j}^{\mathrm{r}}}{\partial T}$ for each chemical reaction j that takes place at the interface;
  - Joule heating due to electrical potential gradient in the solid: $q_{\mathrm{s}}^{\mathrm{r}} = \sigma_{\mathrm{eff}}^{\mathrm{r}} (\nabla \phi_{\mathrm{s}}^{\mathrm{r}} \cdot \nabla \phi_{\mathrm{s}}^{\mathrm{r}})$;
  - Joule heating due to electrochemical potential gradient in the electrolyte: $q_{\mathrm{e}}^{\mathrm{r}} = \kappa_{\mathrm{eff}}^{\mathrm{r}} (\nabla \phi_{\mathrm{e}}^{\mathrm{r}} \cdot \nabla \phi_{\mathrm{e}}^{\mathrm{r}}) + \kappa_{\mathrm{D,eff}}^{\mathrm{r}} (\nabla \ln c_{\mathrm{e}}^{\mathrm{r}} \cdot \nabla \phi_{\mathrm{e}}^{\mathrm{r}})$;
  - Heat generation due to contact resistance, $q_{\mathrm{c}}^{\mathrm{r}} = i_{\mathrm{app}}^2 R_{\mathrm{c}}^{\mathrm{r}}$.[8]

- Following the method from Ch. 1, we can convert Eq. (6.1) into a lumped-parameter version.

- The net operation multiplies both sides of the equation by AL^{r}, giving:

$$\frac{\partial (\bar{c}^{\mathrm{r}} T^{\mathrm{r}})}{\partial t} = \nabla \cdot (\bar{\lambda}^{\mathrm{r}} \nabla T^{\mathrm{r}}) + \bar{q}^{\mathrm{r}},$$

  where T^{r} is still in kelvin, and heat generation $\bar{q}^{\mathrm{r}}$ is in watts.

- In the following, we assume a single reaction at the interface, but this can be regeneralized to multiple reactions if desired.

[8] Note the different units: q_{c} applies only to the current collector/electrode contact region and is specified per unit area, $\mathrm{W\,m^{-2}}$, rather than per unit volume.

- The irreversible heat generation due to de-/intercalation of lithium is written in lumped-parameter form as (where $\mathrm{r} \in \{\mathrm{n}, \mathrm{p}\}$):

$$\bar{q}_{\mathrm{i}}^{\mathrm{r}} = i_{\mathrm{f}}^{\mathrm{r}} \eta^{\mathrm{r}}. \tag{6.2}$$

- The reversible heat generation due to a change in entropy during de-/intercalation is:

$$\bar{q}_{\mathrm{r}}^{\mathrm{r}} = i_{\mathrm{f}}^{\mathrm{r}} T \frac{\partial U_{\mathrm{ocp}}^{\mathrm{r}}}{\partial T}, \tag{6.3}$$

  where $\mathrm{r} \in \{\mathrm{n}, \mathrm{p}\}$ and $\partial U_{\mathrm{ocp}}^{\mathrm{r}} / \partial T$ is the partial molar entropy term that relates changes in $U_{\mathrm{ocp}}^{\mathrm{r}}$ to changes in temperature.

- The heat generation due to polarization caused by the ionic resistance of the electrolyte is written as:

$$\bar{q}_{\mathrm{e}}^{\mathrm{r}} = \bar{\kappa}^{\mathrm{r}} \left(\nabla_{\tilde{x}} \phi_{\mathrm{e}}^{\mathrm{r}} \cdot \nabla_{\tilde{x}} \phi_{\mathrm{e}}^{\mathrm{r}} \right) + \bar{\kappa}^{\mathrm{r}} \bar{\kappa}_D T \left(\nabla_{\tilde{x}} \ln \theta_{\mathrm{e}}^{\mathrm{r}} \cdot \nabla_{\tilde{x}} \phi_{\mathrm{e}}^{\mathrm{r}} \right), \tag{6.4}$$

  where $\mathrm{r} \in \{\mathrm{n}, \mathrm{s}, \mathrm{p}\}$, and the heat generation due to polarization of the electronic resistance of the solid material is written as:

$$\bar{q}_{\mathrm{s}} = \bar{\sigma}^{\mathrm{r}} \left(\nabla_{\tilde{x}} \phi_{\mathrm{s}}^{\mathrm{r}} \cdot \nabla_{\tilde{x}} \phi_{\mathrm{s}}^{\mathrm{r}} \right). \tag{6.5}$$

- Finally, heat generation due to the polarization caused by contact resistance between the current collectors and active material is:

$$\bar{q}_{\mathrm{c}} = R_{\mathrm{c}} i_{\mathrm{app}}^2.$$

- We adopt a simplified form of the heat-flux model, as illustrated, which models the temperature evolution caused by the internal heat generated during discharge and charge processes at only two points: at the cell core and surface.

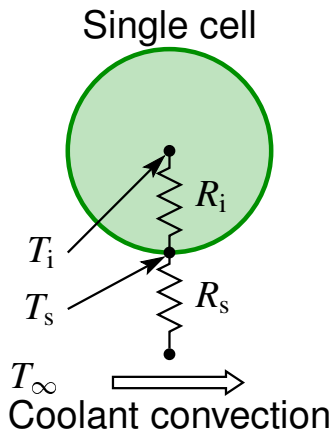

- This model makes the further simplifying assumptions that the internal and surface temperatures are uniform and the heat generation is uniformly distributed within the cell jelly roll.
- The simplified lumped thermal model is described as follows:

$$C_{\mathrm{i}}\frac{\mathrm{d}T_{\mathrm{i}}}{\mathrm{d}t} = \bar{q} + \frac{(T_{\mathrm{s}} - T_{\mathrm{i}})}{R_{\mathrm{i}}} \tag{6.6}$$

$$C_{\mathrm{s}}\frac{\mathrm{d}T_{\mathrm{s}}}{\mathrm{d}t} = \frac{(T_{\mathrm{i}} - T_{\mathrm{s}})}{R_{\mathrm{i}}} + \frac{(T_{\infty} - T_{\mathrm{s}})}{R_{\mathrm{s}}}, \tag{6.7}$$

  where T_{i}, T_{s}, and T_{∞} are the internal core temperature, the surface temperature, and the ambient cooling temperatures.[9]
- C_{i}, C_{s} are lumped cell internal and surface heat capacities; R_{i} is the thermal resistance between cell core and surface; R_{s} is thermal resistance between cell surface and ambient environment.
- Since our interest is in an embedded-processing BMS application, we convert Eqs. (6.6) and (6.7) into a discrete-time state-space form:[10]

$$\begin{bmatrix} T_{\mathrm{i}}[k+1] \\ T_{\mathrm{s}}[k+1] \end{bmatrix} = \begin{bmatrix} \left(1 - \dfrac{\Delta t}{R_{\mathrm{i}}C_{\mathrm{i}}}\right) & \dfrac{\Delta t}{R_{\mathrm{i}}C_{\mathrm{i}}} \\ \dfrac{\Delta t}{R_{\mathrm{i}}C_{\mathrm{s}}} & \left(1 - \dfrac{(R_{\mathrm{i}} + R_{\mathrm{s}})\,\Delta t}{R_{\mathrm{i}}R_{\mathrm{s}}C_{\mathrm{s}}}\right) \end{bmatrix} \begin{bmatrix} T_{\mathrm{i}}[k] \\ T_{\mathrm{s}}[k] \end{bmatrix} + \begin{bmatrix} \dfrac{\Delta t}{C_{\mathrm{i}}} & 0 \\ 0 & \dfrac{\Delta t}{R_{\mathrm{s}}C_{\mathrm{s}}} \end{bmatrix} \begin{bmatrix} \bar{q}[k] \\ T_{\infty}[k] \end{bmatrix}. \tag{6.8}$$

- Parameter temperature-dependence is implemented using the Arrhenius relationship, as discussed in Ch. 3.

[9] This notation T_{s} for surface temperature conflicts with our prior notation for sample period. In this section, sample period is now written as Δt.

[10] Thermal dynamics are slow enough that we use a simple Euler derivative approximation to convert from continuous-time to discrete-time.

6.9: Physics-based reduced-order thermal simulations

- Eq. (6.8) is in a form that can be implemented directly in a BMS.
- It remains only to find a way to compute the heat-generation rate $\bar{q}[k]$ using computed values from the LPM.
- The ROM already implements the variables of Eqs. (6.2) and (6.3); they simply need to be multiplied together to compute of $\bar{q}_{\mathrm{i}}$ and $\bar{q}_{\mathrm{r}}$.
- However, to compute Eqs. (6.4) and (6.5), we require knowledge of the gradients of ϕ_{e}, ϕ_{s}, and $\ln(\theta_{\mathrm{e}})$. To find these:
  - We develop TFs for these gradients (cf. App. 6.b) and use an xRA to convert the TFs to a state-space form for real-time evaluation.

Simulation results and discussion

- We are now present results from a time-domain simulation of the 1D reduced-order thermal model versus a FOM simulated in COMSOL.
- ROM and FOM were fully coupled: present temperature is fed back to modify the temperature-dependent parameters for future times.

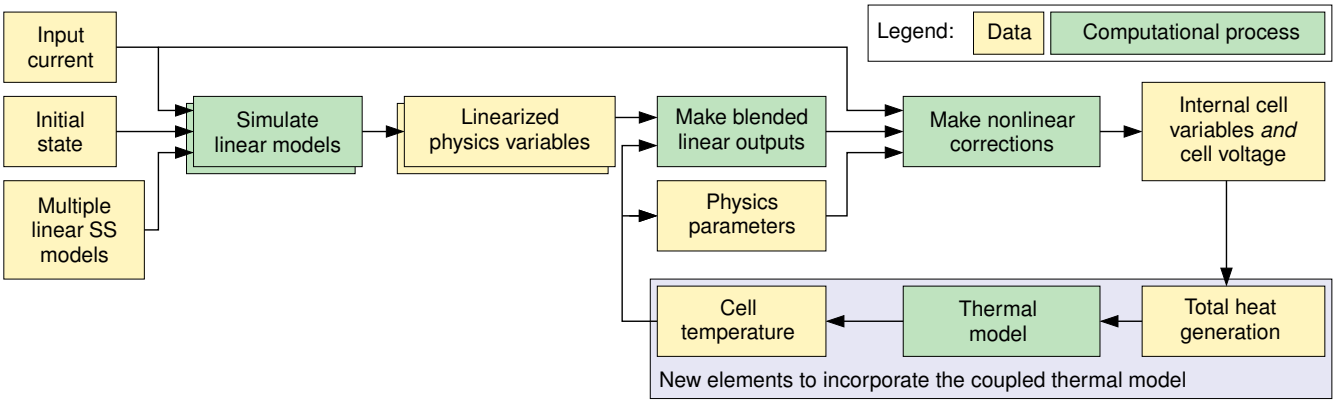

- A set of 8th-order ROMs was created in 2 % SOC and 10 °C temperature increments using the HRA for the NMC30 cell.
- Heat-generation ROMs were created for the same setpoints at intervals of $\Delta\tilde{x} = 0.2$ within the three cell regions.

- Simulations employed output blending and used New York city cycle (NYCC) profile, discharging the cell from 95 % to about 75 % SOC.
- FOM/ROM cell-level-variable predictions appear below:[11]

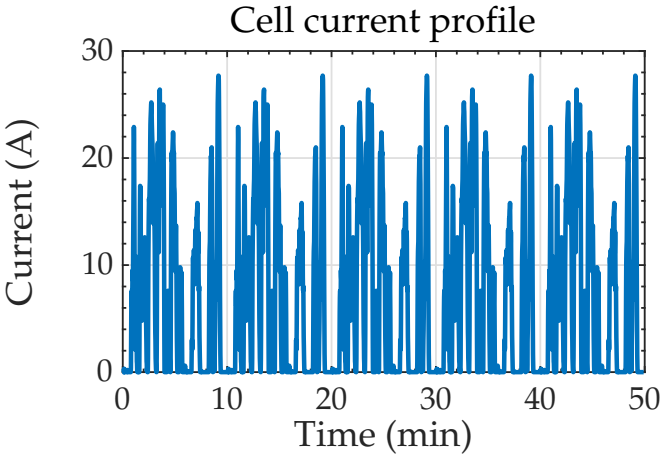

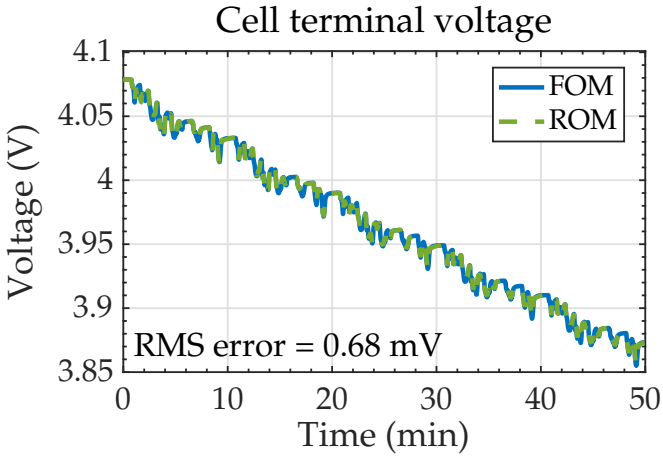

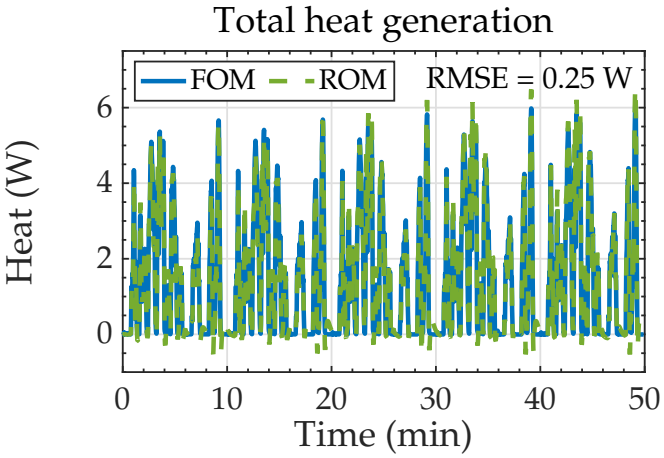

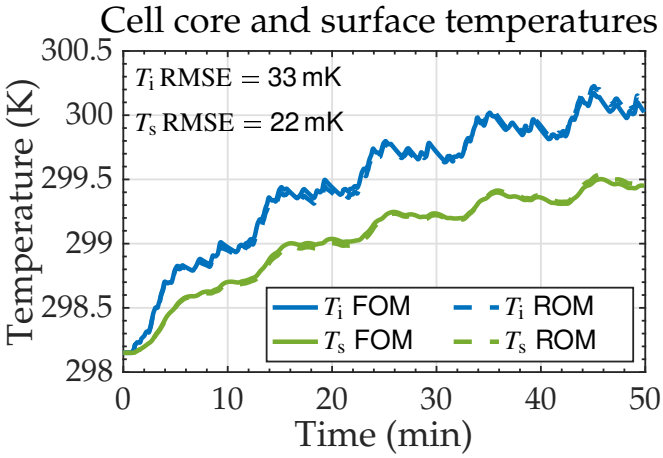

- FOM/ROM individual average heat-generation terms in neg. are:

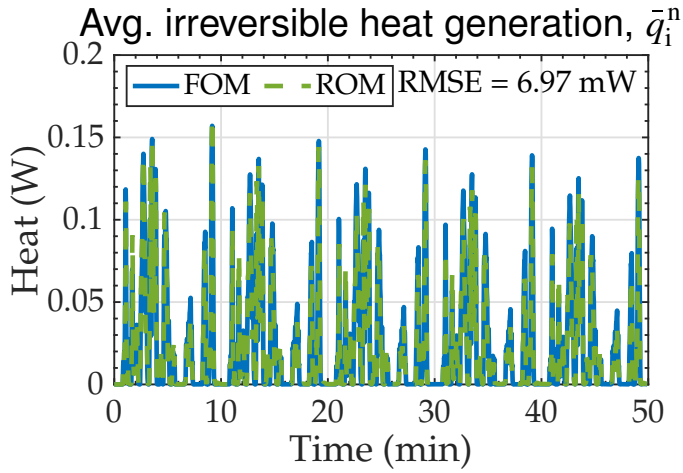

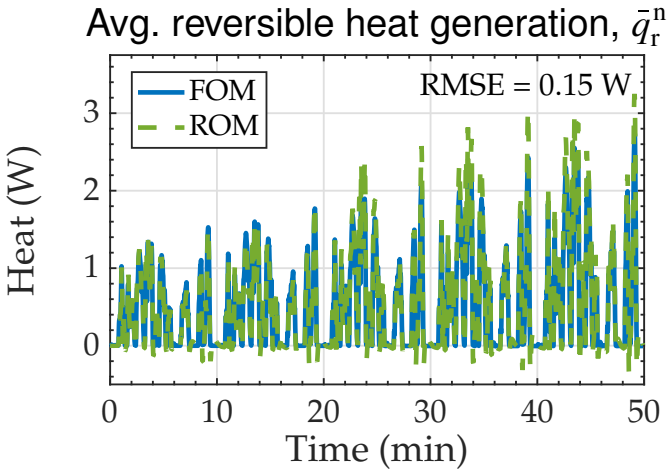

[11] Total heat-generation rate in the figure is the sum of the average heat-generation rate terms calculated using Eq. (6.12) and is the input to Eq. (6.8).

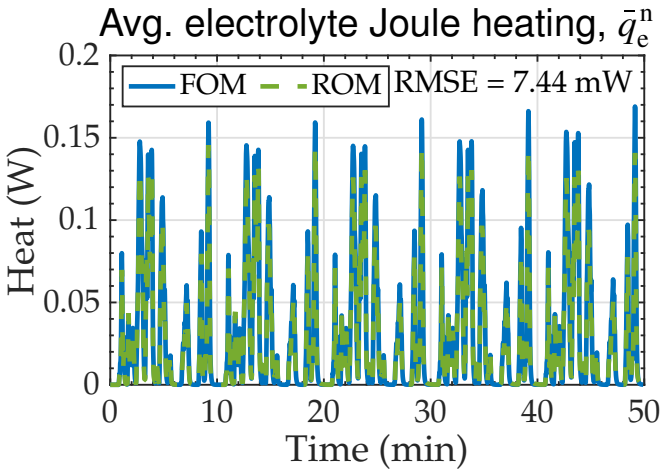

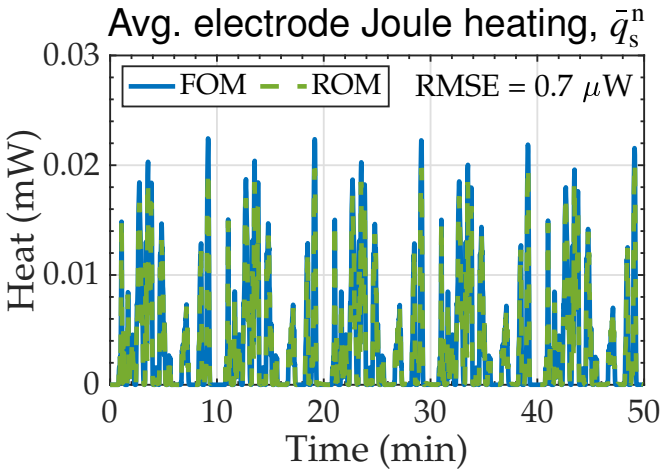

- FOM/ROM individual average heat-generation terms in pos. are:

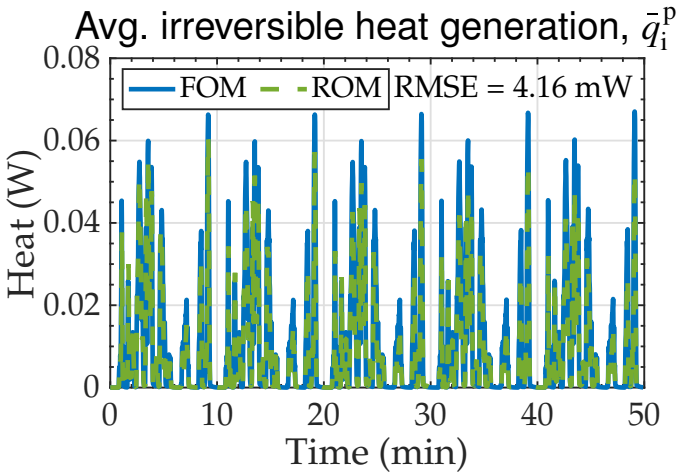

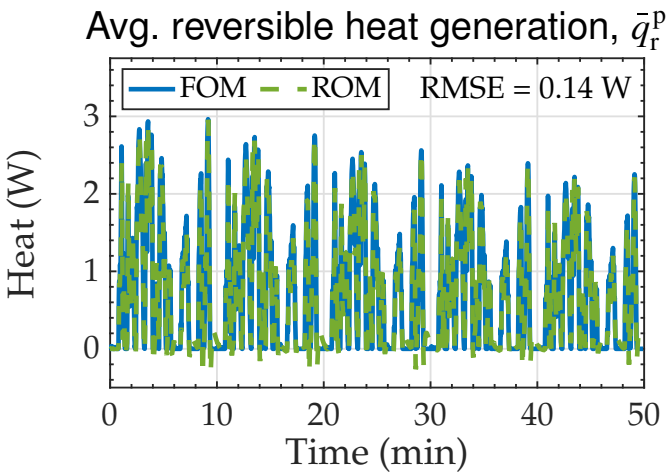

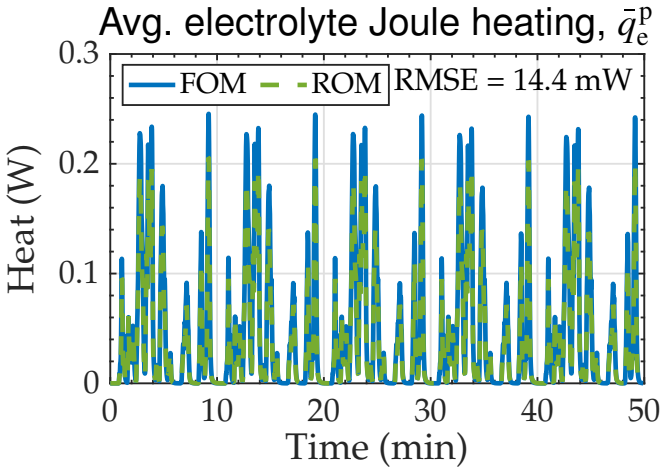

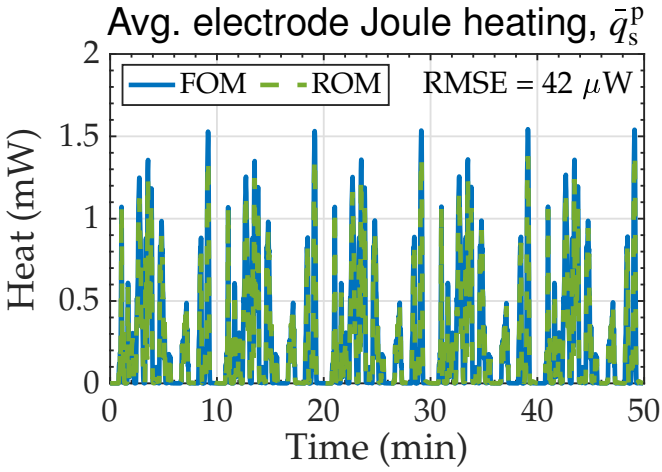

- $\bar{q}_{\mathrm{i}}$, $\bar{q}_{\mathrm{e}}$, and $\bar{q}_{\mathrm{r}}$ are the main contributors to temperature rise; $\bar{q}_{\mathrm{s}}$ is comparatively small and its contributions can probably be neglected.
- Overall, we conclude that the coupled electrochemical/thermal ROM does a good job of predicting both voltage and temperature.

6.10: Cell degradation models

- Another type of prognostic predicts near-future degradation that would occur if some proposed input were to be applied to the cell.
- Topic 6.2 mentioned known Li-ion degradation mechanisms, but not all have been modeled, and their interactions are not well understood.
- Fortunately, we are beginning to see accelerated publication of quantitative physics-based models of Li-ion degradation mechanisms.
- Some of these are illustrated in the figure below; includes LLI via SEI-layer growth and Li plating and LAM via various mechanisms.

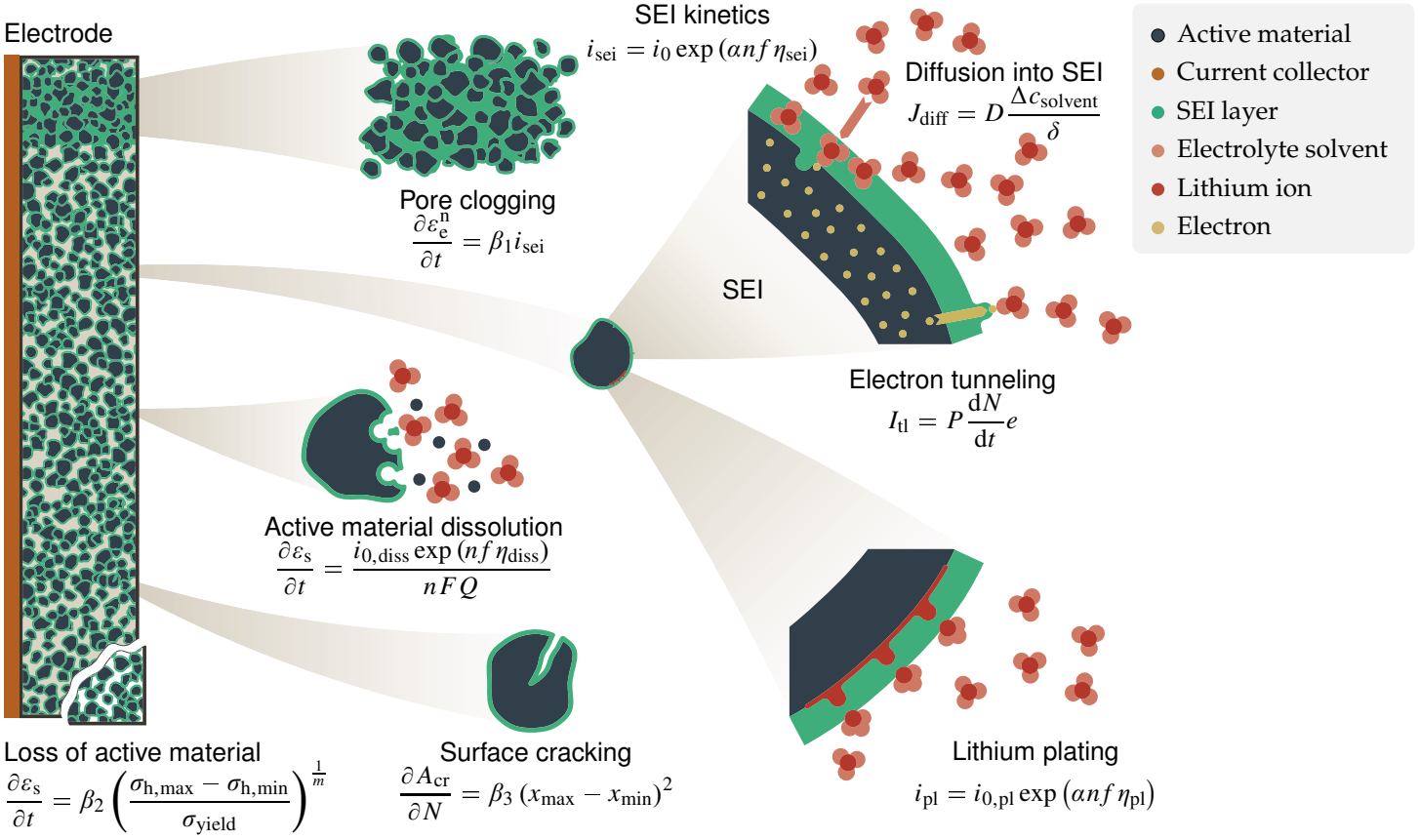

- Whenever we encounter a new model of a degradation mechanism that we would like to implement for BMS prognostics, we must:
  - First convert that model to a lumped-parameter form,
  - Then, simplify the model to be implementable in a BMS, and

  - Finally identify the parameter values of the model.
- In the following, we will illustrate this process with an example.

Full-order model of SEI layer growth

- SEI comprises two distinct parts, an inner layer and outer layer.
- The inner layer is composed of inorganic salts which form a dense structure on the electrode surface, while the outer layer is composed of organic lithium salts which have a highly porous structure.
- Solvent molecules are able to diffuse through the outer layer but cannot penetrate the inner layer.
- The inner layer is a good insulator, but electrons can tunnel from electrode surface to boundary between SEI layers if inner layer is thin.
- The solvent is reduced when electrons and solvent molecules arrive at the boundary together, forming additional dense and porous SEI. Both layers continue to grow over time.
- Different models of SEI-layer growth, making different assumptions regarding the rate-limiting process, are illustrated on the prior page.
  - Ramadass et al. assumed that the reaction kinetics between electrons and solvent limited the rate of growth;
  - Safari et al. assumed that diffusion of the solvent through the outer layer was the limiting factor; and
  - Li et al. assumed that electron tunneling was the rate-limiting term.
- In ECE5720, you learned how to make a 0D approximation to the Ramadass model; we use that work here as an example of the process required to convert a literature aging model for BMS use.

- As a review, the local intercalation reaction rate must be modified to include an extra rate variable modeling the side reaction.
  - The total intercalation current $i^{\mathrm{r}}_{\mathrm{f+s}}(\tilde{x},t)$ is given by a sum of the faradaic rate and the side-reaction rate: $i^{\mathrm{r}}_{\mathrm{f+s}}(\tilde{x},t) = i^{\mathrm{r}}_{\mathrm{f}}(\tilde{x},t) + i^{\mathrm{r}}_{\mathrm{s}}(\tilde{x},t)$.
  - In this equation, $i^{\mathrm{n}}_{\mathrm{s}}(\tilde{x},t) \leq 0$ and we assume that $i^{\mathrm{p}}_{\mathrm{s}}(\tilde{x},t) = 0$.
- Recall, $i^{\mathrm{r}}_{\mathrm{f}}(\tilde{x},t)$ is faradaic flux modeled via the MSMR equation:

$$
\begin{aligned}
i^{\mathrm{r}}_{\mathrm{f}}(\tilde{x},t) &= \textstyle\sum_{j=1}^{J^{\mathrm{r}}} i^{\mathrm{r}}_{\mathrm{f},j}(\tilde{x},t) \\
i^{\mathrm{r}}_{\mathrm{f},j}(\tilde{x},t) &= i^{\mathrm{r}}_{0,j}(\tilde{x},t)\left(\exp\left((1-\alpha^{\mathrm{r}}_j) f \eta^{\mathrm{r}}(\tilde{x},t)\right) - \exp\left(-\alpha^{\mathrm{r}}_j f \eta^{\mathrm{r}}(\tilde{x},t)\right)\right) \\
i^{\mathrm{r}}_{0,j}(\tilde{x},t) &= \bar{k}^{\mathrm{r}}_{0,j}\left(X^{\mathrm{r}}_j - x^{\mathrm{r}}_j(\tilde{x},t)\right)^{\omega^{\mathrm{r}}_j(1-\alpha^{\mathrm{r}}_j)}\left(x^{\mathrm{r}}_j(\tilde{x},t)\right)^{\omega^{\mathrm{r}}_j\alpha^{\mathrm{r}}_j}\left(\theta^{\mathrm{r}}_{\mathrm{e}}(\tilde{x},t)\right)^{1-\alpha^{\mathrm{r}}_j} \\
\eta^{\mathrm{r}}(\tilde{x},t) &= \phi^{\mathrm{r}}_{\mathrm{s}}(\tilde{x},t) - \phi^{\mathrm{r}}_{\mathrm{e}}(\tilde{x},t) - U^{\mathrm{r}}_{\mathrm{ocp}}\left(\theta^{\mathrm{r}}_{\mathrm{ss}}(\tilde{x},t)\right) - \bar{R}^{\mathrm{r}}_{\mathrm{f}} i^{\mathrm{r}}_{\mathrm{f+dl}}(\tilde{x},t).
\end{aligned}
$$

- The kinetics of the side reaction are assumed to be irreversible and are described using a Tafel equation:[12]

$$
\begin{aligned}
i^{\mathrm{n}}_{\mathrm{s}}(\tilde{x},t) &= -\bar{i}_{\mathrm{s},0}\exp\left(-\alpha_{\mathrm{s}} f \eta^{\mathrm{n}}_{\mathrm{s}}(\tilde{x},t)\right) \\
\eta^{\mathrm{n}}_{\mathrm{s}}(\tilde{x},t) &= \phi^{\mathrm{n}}_{\mathrm{s}}(\tilde{x},t) - \phi^{\mathrm{n}}_{\mathrm{e}}(\tilde{x},t) - U_{\mathrm{s}} - \bar{R}^{\mathrm{n}}_{\mathrm{f}} i^{\mathrm{n}}_{\mathrm{f+s}}(\tilde{x},t),
\end{aligned}
\tag{6.9}
$$

  where $\bar{i}_{\mathrm{s},0}$ is side-reaction exchange rate, U_{s} is side-reaction potential, and α_{s} is a unitless (cathodic) transfer coefficient for solvent reduction.
- Note that we assume there is only one reaction that forms the SEI layer instead of considering multiple galleries j.

Eliminating redundant parameters

- In this model, two key parameters, $\bar{i}_{\mathrm{s},0}$ and U_{s}, turn out not to be independently identifiable.

[12] The superscripts "n" on the three SEI-model parameters are omitted because they are negative-electrode quantities by default.

- To see this, substitute the overpotential term $\eta_{\mathrm{s}}^{\mathrm{n}}(\tilde{x},t)$ into Eq. (6.9):

$$\begin{aligned} i_{\mathrm{s}}^{\mathrm{n}}(\tilde{x},t) &= -\bar{i}_{\mathrm{s},0}\exp\left(-\alpha_{\mathrm{s}} f\left(\phi_{\mathrm{s}}^{\mathrm{n}}(\tilde{x},t)-\phi_{\mathrm{e}}^{\mathrm{n}}(\tilde{x},t)-U_{\mathrm{s}}-\bar{R}_{\mathrm{f}}^{\mathrm{n}} i_{\mathrm{f+s}}^{\mathrm{n}}(\tilde{x},t)\right)\right) \\ &= -\underbrace{\left[\bar{i}_{\mathrm{s},0}\exp\left(\alpha_{\mathrm{s}} f U_{\mathrm{s}}\right)\right]}_{\bar{k}_{\mathrm{s},0}(T)}\exp\left(-\alpha_{\mathrm{s}} f\left(\phi_{\mathrm{s}}^{\mathrm{n}}(\tilde{x},t)-\phi_{\mathrm{e}}^{\mathrm{n}}(\tilde{x},t)-\bar{R}_{\mathrm{f}}^{\mathrm{n}} i_{\mathrm{f+s}}^{\mathrm{n}}(\tilde{x},t)\right)\right). \end{aligned}$$

- We explore the term in the square brackets, assuming Arrhenius temperature-dependence for $\bar{i}_{\mathrm{s},0}$, expanding $f = F/(RT)$ for clarity:

$$\begin{aligned} \bar{k}_{\mathrm{s},0}(T) &= \bar{i}_{\mathrm{s},0,\mathrm{ref}}\exp\left(\frac{\alpha_{\mathrm{s}} F}{RT}U_{\mathrm{s}}\right)\exp\left(\frac{E_{\bar{i}_{\mathrm{s},0}}}{R}\left(\frac{1}{T_{\mathrm{ref}}}-\frac{1}{T}\right)\right) \\ &= \bar{i}_{\mathrm{s},0,\mathrm{ref}}\exp\left(\frac{E_{\bar{i}_{\mathrm{s},0}}}{R}\left(\frac{1}{T_{\mathrm{ref}}}-\frac{1}{T}\right)+\frac{\alpha_{\mathrm{s}} F}{RT}U_{\mathrm{s}}+\frac{\alpha_{\mathrm{s}} F}{RT_{\mathrm{ref}}}U_{\mathrm{s}}-\frac{\alpha_{\mathrm{s}} F}{RT_{\mathrm{ref}}}U_{\mathrm{s}}\right) \\ &= \bar{i}_{\mathrm{s},0,\mathrm{ref}}\exp\left(\frac{\alpha_{\mathrm{s}} F}{RT_{\mathrm{ref}}}U_{\mathrm{s}}\right)\exp\left(\frac{E_{\bar{i}_{\mathrm{s},0}}}{R}\left(\frac{1}{T_{\mathrm{ref}}}-\frac{1}{T}\right)-\frac{\alpha_{\mathrm{s}} F U_{\mathrm{s}}}{R}\left(\frac{1}{T_{\mathrm{ref}}}-\frac{1}{T}\right)\right) \\ &= \underbrace{\bar{i}_{\mathrm{s},0,\mathrm{ref}}\exp\left(\frac{\alpha_{\mathrm{s}} F}{RT_{\mathrm{ref}}}U_{\mathrm{s}}\right)}_{\bar{k}_{\mathrm{s},0,\mathrm{ref}}}\exp\left(\frac{\overbrace{\left(E_{\bar{i}_{\mathrm{s},0}}-\alpha_{\mathrm{s}} F U_{\mathrm{s}}\right)}^{E_{\bar{k}_{\mathrm{s},0}}}}{R}\left(\frac{1}{T_{\mathrm{ref}}}-\frac{1}{T}\right)\right). \end{aligned}$$

- Overall, independent definitions of $\bar{i}_{\mathrm{s},0}$ and U_{s} can now be completely ignored, and the Tafel equation is reformulated as:

$$\begin{aligned} i_{\mathrm{s}}^{\mathrm{n}}(\tilde{x},t) &= -\bar{k}_{\mathrm{s},0}\exp\left(-\alpha_{\mathrm{s}} f\left(\phi_{\mathrm{s}}^{\mathrm{n}}(\tilde{x},t)-\phi_{\mathrm{e}}^{\mathrm{n}}(\tilde{x},t)-\bar{R}_{\mathrm{f}}^{\mathrm{n}} i_{\mathrm{f+s}}^{\mathrm{n}}(\tilde{x},t)\right)\right) \\ \bar{k}_{\mathrm{s},0} &= \bar{k}_{\mathrm{s},0,\mathrm{ref}}\exp\left(\frac{E_{\bar{k}_{\mathrm{s},0}}}{R}\left(\frac{1}{T_{\mathrm{ref}}}-\frac{1}{T}\right)\right). \end{aligned}$$

- Aging experiments must then be designed to expose three parameters in the negative-electrode: $\bar{k}_{\mathrm{s},0}$, $E_{\bar{k}_{\mathrm{s},0}}$, and α_{s}.
- Next, we will reformulate the time-domain models and create a reduced-order structure by making several assumptions.

An algebraic solution for $i_{\rm s}(t) \approx i_{\rm s}(\tilde{x}, t)$

- We simplify the model the same way as presented in ECE5720.
- We first make three assumptions in addition to those of Ramadass:
  1. The anodic and cathodic charge-transfer coefficients of the intercalation and side reactions are all equal ($\alpha_j^{\rm n} = \alpha_j^{\rm p} = \alpha_{\rm s} = 0.5$).
  2. The cell is always in a quasi-equilibrium state, allowing the intercalation reaction rate constant $i_{0,j}^{\rm r}(\tilde{x}, t)$ to be approximated by:

$$i_{0,j}^{\rm r}(\tilde{x}, t) \approx i_{0,j}^{\rm r}(t) = \bar{k}_{0,j}^{\rm r} \sqrt{(X_j^{\rm r} - x_j^{\rm r}(t))^{\omega_j^{\rm r}} (x_j^{\rm r}(t))^{\omega_j^{\rm r}}(1)}$$

$$x_j^{\rm r}(t) = \frac{X_j^{\rm r}}{1 + \exp[f(U_{\rm ocp}\left(\theta_{\rm ss}^{\rm r}(t)\right) - U_j^{0,{\rm r}})/\omega_j^{\rm r}]},$$

     where $\theta_{\rm e}^{\rm r}(\tilde{x}, t) \approx \theta_{{\rm e},0}^{\rm r} = 1$.
  3. Intercalation (faradaic) rate $i_{\rm f}^{\rm r}(\tilde{x}, t)$ and side-reaction rate $i_{\rm s}^{\rm r}(\tilde{x}, t)$ are uniform over the electrode for a small time interval Δt, where the values are given by $i_{\rm f}^{\rm r}[k]$ and $i_{\rm s}^{\rm r}[k]$ at the kth discrete-time interval. This allows us to write the total interfacial rate $i_{\rm f+s}^{\rm r}[k]$ as:

$$i_{\rm f+s}^{\rm n}[k] = i_{\rm f}^{\rm n}[k] + i_{\rm s}^{\rm n}[k] = i_{\rm app}[k], \quad \text{and} \quad i_{\rm f+s}^{\rm p}[k] = i_{\rm f}^{\rm p}[k] = -i_{\rm app}[k].$$

- With the above assumptions, a reduced-order degradation model is readily formulated (again, omitting superscript "n" for brevity).
- First, recall that $i_{\rm f}(\tilde{x}, t)$ is represented by the MSMR model; based on Assumption 1, we find the overpotential as:

$$i_{\rm f}(\tilde{x}, t) = \sum_{j=1}^{J} i_{0,j}(\tilde{x}, t) \left\{ \exp\left(\frac{f}{2}\eta(\tilde{x}, t)\right) - \exp\left(\frac{-f}{2}\eta(\tilde{x}, t)\right) \right\}$$

$$= 2\sum_{j=1}^{J} i_{0,j}(\tilde{x}, t) \sinh\left(\frac{f}{2}\eta(\tilde{x}, t)\right)$$

$$\eta(\tilde{x},t) = \frac{2}{f}\text{asinh}\left(\frac{i_\text{f}(\tilde{x},t)}{2\sum i_{0,j}(\tilde{x},t)}\right).$$

- The side-reaction and intercalation overpotentials can be related:

$$\begin{aligned}\eta(\tilde{x},t) &= \left[\phi_\text{s}(\tilde{x},t) - \phi_\text{e}(\tilde{x},t) - \bar{R}_\text{f} i_\text{f+s}(\tilde{x},t)\right] - U_\text{ocp}\left(\theta_\text{ss}(\tilde{x},t)\right)\\ \eta_\text{s}(\tilde{x},t) &= \phi_\text{s}^\text{n}(\tilde{x},t) - \phi_\text{e}^\text{n}(\tilde{x},t) - \bar{R}_\text{f}^\text{n} i_\text{f+s}^\text{n}(\tilde{x},t)\\ &= \eta(\tilde{x},t) + U_\text{ocp}\left(\theta_\text{ss}(\tilde{x},t)\right).\end{aligned}$$

- Therefore, the side-reaction rate can be written as:

$$\begin{aligned}i_\text{s}(\tilde{x},t) &= -\bar{k}_{\text{s},0}\exp\left(-\frac{f}{2}\left(\eta(\tilde{x},t) + U_\text{ocp}\left(\theta_\text{ss}(\tilde{x},t)\right)\right)\right)\\ &= -\bar{k}_{\text{s},0}\exp\left(\text{asinh}\left(\frac{-i_\text{f}(\tilde{x},t)}{2\sum i_{0,j}(\tilde{x},t)}\right) - \frac{f}{2}U_\text{ocp}\left(\theta_\text{ss}(\tilde{x},t)\right)\right). \quad (6.10)\end{aligned}$$

- The film resistance and solid/electrolyte potentials cancel from the calculation, which infers that we don't need the full ideal-cell LPM in order to simulate the side reactions.

- Implementing Assumption 3 and rearranging Eq. (6.10):

$$\begin{aligned}i_\text{s}(\tilde{x},t) &= -\bar{k}_{\text{s},0}\exp\left(\text{asinh}\left(\frac{i_\text{s}(\tilde{x},t) - i_\text{app}}{2\sum i_{0,j}(\tilde{x},t)}\right) - \frac{f}{2}U_\text{ocp}\left(\theta_\text{ss}(\tilde{x},t)\right)\right)\\ &= -\bar{k}_{\text{s},0}\exp\left(\text{asinh}\left(\frac{-i_\text{app}}{2\sum i_{0,j}(\tilde{x},t)} + \frac{1}{2\sum i_{0,j}(\tilde{x},t)} i_\text{s}(\tilde{x},t)\right)\right.\\ &\qquad\left. - \frac{f}{2}U_\text{ocp}(\theta_\text{ss}(\tilde{x},t))\right).\end{aligned}$$

- If we assume that local variations for all variables can be ignored,

$$i_{0,j}(\tilde{x},t) \approx i_{0,j}(t), \quad i_\text{s}(\tilde{x},t) \approx i_\text{s}(t), \quad \text{and} \quad \theta_\text{ss}(\tilde{x},t) \approx \theta_\text{ss}(t).$$

- We consider each variable to be constant over sample period Δt, where the value is denoted as, for example, $i_\text{s}[k]$ for the kth interval.

- Subsequently, the continuous-time formulation is then converted to discrete time as (we let $i_0[k] = \sum i_{0,j}[k]$):

$$i_s[k] = -\bar{k}_{s,0} \exp\left(\text{asinh}\left(\frac{-i_{app}[k]}{2i_0[k]} + \frac{i_s[k]}{2i_0[k]}\right) - \frac{f}{2} U_{ocp}\left(\theta_{ss}[k]\right)\right). \quad (6.11)$$

- This equation is implicit since $i_s[k]$ appears on both sides.
- We solve for $i_s[k]$ using the same method used in ECE5720. The key identity that helps to simplify the formula is:

$$\exp\left(\text{asinh}\left(x\right)\right) = x + \sqrt{x^2+1},$$

  and a quadratic form of Eq. (6.11) is then revealed.
- The root is easily solved by adopting the quadratic formula.
- Deviation details are omitted here (they are in ECE5720 notes).
- Only the final algebraic result is shown:

$$i_s[k] = A \exp\left(\text{asinh}\left(B + C i_s[k]\right)\right) = \frac{AB + A\sqrt{B^2 + (1-2CA)}}{1-2CA},$$

  where,

$$i_0[k] = \sum i_{0,j}[k] = \sum \bar{k}_{0,j} \sqrt{\left(X_j - x_j[k]\right)^{\omega_j} \left(x_j[k]\right)^{\omega_j}}$$

$$x_j[k] = \frac{X_j}{1 + \exp[f\left(U_{ocp}\left(\theta_{ss}[k]\right) - U_j^0\right)/\omega_j]}$$

$$A = -\bar{k}_{s,0} \exp\left(-\frac{f}{2} U_{ocp}\left(\theta_{ss}[k]\right)\right), \quad B = -\frac{i_{app}[k]}{2i_0[k]}, \quad C = \frac{1}{2i_0[k]}.$$

- To simulate $i_s[k]$ the following parameters are required:
  1. Universal constants F and R, and
  2. Intercalation and side-reaction rate constants $\bar{k}^n_{0,j}$ and $\bar{k}_{s,0}$.

- The variables needed to compute the time-varying output are:
  1. Temperature T,
  2. Applied current $i_{\text{app},k}$,
  3. The negative-electrode OCP function $U^{\text{n}}_{\text{ocp}}$, and
  4. The negative-electrode surface stoichiometry $\theta^{\text{n}}_{\text{ss}}[k]$.

Identifying SEI model parameter values

- We have now reformulated the Ramadass SEI model to eliminate redundant parameters and have simplified it to a 0D ROM.
- Before we implement this model, we must still estimate $\bar{k}_{\text{s},0}$ and $E_{\bar{k}_{\text{s},0}}$.
- These constants may be found by conducting calendar-life tests at different temperatures and periodically measuring lost capacity via a full calibrated discharge and charge cycle.
- Subtle point: summing the lithium ion loss predicted by $i_{\text{s}}[k]$ over time is not the same as the measured total-capacity loss—some capacity is recovered by shifts in electrode stoichiometric operating windows.
- It is also possible to use voltage measurements during calendar-life tests to verify the applicability of the Ramadass, Safari, or Li methods.
  - However, cell voltage does not decrease due to SEI side-reactions alone, and this must be taken into account.
  - Lu et al. discuss these issues in detail, including how to estimate the SEI model parameter values from calendar-life data.[13]

[13] Lu, D., Trimboli, M.S., Wang, Y., Plett, G.L., "Modeling Voltage Decay During Calendar-Life Aging," *Journal of the Electrochemical Society*, 169(12), 2022, 120515.

Where to from here?

- This chapter has provided a high-level survey of some important topics in cell diagnosis and prognosis.
- This field is rapidly evolving, and high-quality articles are being published at an accelerating rate by researchers around the world.
- There remains a need to improve the speed, accuracy, robustness, and specificity of diagnostics, and to validate the results.
- There is also a need to expand the number of degradation mechanisms that are modeled to improve prognosis.
- Physics-based models are required to do both of these well.
  - O'Kane et al. write, "Empirical models may capture [degradation] behavior, but they can offer insights into how to prevent degradation only when combined with physics-based models."
- Another significant omission in the literature is advice regarding how to combine the models of different degradation mechanisms when their effects are known to be coupled.
- The only article of which we are aware that makes an attempt to do so is the work by O'Kane et al.
- We look forward to seeing more works like this in the future.
- However, even the simplified diagnostics and prognostics that we have discussed are a good starting point.
- Chaps. 7–8 will particularly use the prognostics models to inform BMS computations that provide advisory limits of operation during charging and dynamic usage.

Appendix 6.a: Summary of variables

- $\Delta\theta_{\mathrm{s}}^{\mathrm{r}} = \left|\theta_{100}^{\mathrm{r}} - \theta_{0}^{\mathrm{r}}\right|$ [unitless], the range of stoichiometry used in electrode r between SOC of 0 % and 100 %.
- η_{s} [A], side-reaction overpotential.
- i_{s} [A], side-reaction current.
- $\boldsymbol{\Lambda}_j$, the likelihood in the IMM framework of the present voltage measurement given that the cell is described by model j.
- $\boldsymbol{\mu}_i$, the pmf output by the IMM framework summarizing the probability that the cell is best described by model i at the current timestep.
- $\mu_{i|j}$, the conditional probability in the IMM framework of having been in mode i at the prior timestep given that the system is currently in mode j.
- $\boldsymbol{p}_{ij}$, the probability in the IMM framework of transitioning from model i to model j.
- $Q^{\mathrm{r}} = \dfrac{\varepsilon_{\mathrm{s}}^{\mathrm{n}} A L^{\mathrm{n}} c_{\mathrm{s,max}}^{\mathrm{n}} F}{3600}$ [Ah], the theoretical capacity of electrode r, if the entire stoichiometric range from 0 to 1 could be used.
- $\bar{q}^{\mathrm{r}}$ [W], total heat generation in cell region r.
- $\bar{q}_{\mathrm{c}}^{\mathrm{r}}$ [W], heat generation due to contact resistance.
- $\bar{q}_{\mathrm{e}}^{\mathrm{r}}$ [W], Joule heat generation in cell region r in the electrolyte.
- $\bar{q}_{\mathrm{i}}^{\mathrm{r}}$ [W], irreversible heat generation in cell region r.
- $\bar{q}_{\mathrm{r}}^{\mathrm{r}}$ [W], reversible (entropic) heat generation in cell region r.
- $\bar{q}_{\mathrm{s}}^{\mathrm{r}}$ [W], Joule heat generation in the solid (electrode) in cell region r.
- T_{i} [K], temperature at the interior (core) of the cell.
- T_{s} [K], temperature at the surface of the cell.
- T_{∞} [K], ambient temperature.

Appendix 6.b: Gradient TFs for thermal model

- This appendix shows how to compute Eqs. (6.2) and (6.3) if the ROM already produces the required gradient terms; in the following subsection we will show how to derive the necessary gradient TFs.
- We start with the reversible and irreversible heat-generation terms.
- The ROM for irreversible heat generation at the electrode level in the negative and positive electrodes is given by:

$$\bar{q}_{\mathrm{i}}^{\mathrm{r}}[\tilde{x},k] = i_{\mathrm{f}}^{\mathrm{r}}[\tilde{x},k]\eta[x,k],$$

  where, we recall that,[14]

$$\eta^{\mathrm{r}}[\tilde{x},k] = \frac{2}{f}\mathrm{asinh}\left(\frac{i_{\mathrm{f}}^{\mathrm{r}}[\tilde{x},k]}{2\sum_{j=1}^{J^{\mathrm{r}}}\bar{k}_{0,j}^{\mathrm{r}}\sqrt{(X_j^{\mathrm{r}}-x_j^{\mathrm{r}}[\tilde{x},k])^{\omega_j^{\mathrm{r}}}(x_j^{\mathrm{r}}[\tilde{x},k])^{\omega_j^{\mathrm{r}}}\theta_{\mathrm{e}}^{\mathrm{r}}[\tilde{x},k]}}\right).$$

- Similarly, for the reversible heat generation rate term, we have:

$$\bar{q}_{\mathrm{r}}^{\mathrm{r}}[\tilde{x},k] = i_{\mathrm{f}}^{\mathrm{r}}[\tilde{x},k]T_{\mathrm{i}}[k]\frac{\partial U_{\mathrm{ocp}}(\theta_{\mathrm{ss}}^{\mathrm{r}}[\tilde{x},k])}{\partial T},$$

  where temperature $T_{\mathrm{i}}[k]$ is updated every timestep by thermal model.
- Since we have already derived the TFs for several necessary variables—namely, those for $\tilde{\phi}_{\mathrm{s}}$, $\tilde{\phi}_{\mathrm{e}}$, and $\tilde{\theta}_{\mathrm{e}}$—we can find the gradient TFs by taking their derivatives with respect to spatial variable $\tilde{x}$.
- We will show how to do so in the next subsection.
- From the gradient TFs, we use an xRA to implement $\nabla_{\tilde{x}}\tilde{\phi}_{\mathrm{s}}[\tilde{x},k]$, $\nabla_{\tilde{x}}\tilde{\phi}_{\mathrm{e}}[\tilde{x},k]$, and $\nabla_{\tilde{x}}\tilde{\theta}_{\mathrm{e}}[\tilde{x},k]$.

[14] The x_j^{r} are found via the electrode surface potential as a function of $\theta_{\mathrm{ss}}^{\mathrm{r}}$: $U[\tilde{x},k] = U_{\mathrm{ocp}}^{\mathrm{r}}(\theta_{\mathrm{ss}}^{\mathrm{r}}[\tilde{x},k])$. Then we compute: $x_j^{\mathrm{r}}[\tilde{x},k] = X_j^{\mathrm{r}}/\left(1+\exp\left[f(U[\tilde{x},k]-U_j^{0,\mathrm{r}})/\omega_j^{\mathrm{r}}\right]\right)$.

- Notice that we do not mention the $\nabla \ln(\theta_{\mathrm{e}})$ term. See footnote.[15]
- Assuming that these signals are available at the output of the ROM, $\bar{q}_{\mathrm{s}}$ in the negative and positive electrodes is written as:

$$\bar{q}_{\mathrm{s}}^{\mathrm{r}}[\tilde{x}, k] = \bar{\sigma}^{\mathrm{r}} \nabla_{\tilde{x}} \tilde{\phi}_{\mathrm{s}}^{\mathrm{r}}[\tilde{x}, k] \nabla_{\tilde{x}} \tilde{\phi}_{\mathrm{s}}^{\mathrm{r}}[\tilde{x}, k].$$

- Similarly, the ROM for $\bar{q}_{\mathrm{e}}$ at the separator and negative/positive electrodes is written as:

$$\bar{q}_{\mathrm{e}}[\tilde{x}, k] = \bar{\kappa} \left(\nabla_{\tilde{x}} \phi_{\mathrm{e}}[\tilde{x}, k] \nabla_{\tilde{x}} \phi_{\mathrm{e}}[\tilde{x}, k] \right) + \bar{\kappa}_D \left(\nabla_{\tilde{x}} \theta_{\mathrm{e}}[\tilde{x}, k] \nabla_{\tilde{x}} \phi_{\mathrm{e}}[\tilde{x}, k] \right).$$

- We note that so far we have developed ROMs for the heat generation rate terms only for a given spatial location $\tilde{x}$.
- Therefore, in order to calculate the average heat generation rate $\bar{q}[k]$ in the separator and in the negative and positive electrodes, we must generate ROMs at different locations within the cell and then perform integration over the respective region, which yields:

$$\bar{q}_j^{\mathrm{r}}[k] = \int_0^1 \bar{q}_j[z, k] \, \mathrm{d}z$$

where subscript $j \in \{\mathrm{i}, \mathrm{r}, \mathrm{e}, \mathrm{s}\}$ and the spatial variable is normalized using the notation:

$$z = \begin{cases} \tilde{x}, & \text{in the negative electrode} \\ \tilde{x} - 1, & \text{in the separator region} \\ 3 - \tilde{x}, & \text{in the positive electrode.} \end{cases}$$

[15] The debiased lumped electrolyte concentration was previously defined as $\tilde{\theta}_{\mathrm{e}}(\tilde{x}, t) = \theta_{\mathrm{e}}(\tilde{x}, t) - \theta_{\mathrm{e},0}(\tilde{x}, t)$, where $\theta_{\mathrm{e},0}$ is the equilibrium electrolyte concentration, which is equal to 1 in the LPM. Linearizing $\ln(\theta_{\mathrm{e}})$ via Taylor-series expansion gives:

$$\ln(\theta_{\mathrm{e}}(\tilde{x}, t)) = \ln(1 + \tilde{\theta}_{\mathrm{e}}(\tilde{x}, t)) \approx \tilde{\theta}_{\mathrm{e}}(\tilde{x}, t).$$

As a result of linearization, we must instead find $\nabla \ln(\theta_{\mathrm{e}}) \approx \nabla \tilde{\theta}_{\mathrm{e}}(\tilde{x}, s)$.

- Finally, the total heat-generation rate is computed as the sum of the average heat-generation rate terms at each cell region in addition to the Ohmic contact resistance heat generation rate term:

$$\bar{q}[k] = \bar{q}^{\mathrm{n}}[k] + \bar{q}^{\mathrm{s}}[k] + \bar{q}^{\mathrm{p}}[k] + R_{\mathrm{c}} i_{\mathrm{app}}[k], \tag{6.12}$$

  where:

$$\bar{q}^{\mathrm{n}}[k] = \bar{q}^{\mathrm{n}}_{\mathrm{i}}[k] + \bar{q}^{\mathrm{n}}_{\mathrm{r}}[k] + \bar{q}^{\mathrm{n}}_{\mathrm{s}}[k] + \bar{q}^{\mathrm{n}}_{\mathrm{e}}[k]$$

$$\bar{q}^{\mathrm{s}}[k] = \bar{q}^{\mathrm{s}}_{\mathrm{e}}[k]$$

$$\bar{q}^{\mathrm{p}}[k] = \bar{q}^{\mathrm{p}}_{\mathrm{i}}[k] + \bar{q}^{\mathrm{p}}_{\mathrm{r}}[k] + \bar{q}^{\mathrm{p}}_{\mathrm{s}}[k] + \bar{q}^{\mathrm{p}}_{\mathrm{e}}[k].$$

- All that remains to describe the heat-generation model is a derivation of the gradient TFs, which we present here.

Gradient TF of electrolyte stoichiometry, $\nabla_{\tilde{x}} \tilde{\theta}_{\mathrm{e}}$

- The TF of the debiased electrolyte concentration for the cell's electrode regions was given in Ch. 2, which we repeat here:

$$\frac{\widetilde{\Theta}^{\mathrm{r}}_{\mathrm{e}}(z,s)}{I_{\mathrm{app}}(s)} = c^{\mathrm{r}}_1(s) e^{\Lambda^{\mathrm{r}}_1(z-1)} + c^{\mathrm{r}}_2(s) e^{-\Lambda^{\mathrm{r}}_1 z} + c^{\mathrm{r}}_3(s) e^{\Lambda^{\mathrm{r}}_2(z-1)} + c^{\mathrm{r}}_4(s) e^{-\Lambda^{\mathrm{r}}_2 z},$$

  and for the separator region as:

$$\frac{\widetilde{\Theta}^{\mathrm{s}}_{\mathrm{e}}(z,s)}{I_{\mathrm{app}}(s)} = c^{\mathrm{s}}_1(s) e^{\Lambda^{\mathrm{s}}_1(z-1)} + c^{\mathrm{s}}_2(s) e^{-\Lambda^{\mathrm{s}}_1 z}.$$

- Beginning with these, we find the gradient transfer function in the negative electrode, written in terms of spatial variable $\tilde{x}$, to be:

$$\begin{aligned}\frac{\nabla_{\tilde{x}} \widetilde{\Theta}^{\mathrm{n}}_{\mathrm{e}}(\tilde{x},s)}{I_{\mathrm{app}}(s)} &= c^{\mathrm{n}}_1(s)\Lambda^{\mathrm{n}}_1(s) e^{\Lambda^{\mathrm{n}}_1(s)(\tilde{x}-1)} - c^{\mathrm{n}}_2(s)\Lambda^{\mathrm{n}}_1(s) e^{-\Lambda^{\mathrm{n}}_1(s)\tilde{x}} \\ &\quad + c^{\mathrm{n}}_3(s)\Lambda^{\mathrm{n}}_2(s) e^{\Lambda^{\mathrm{n}}_2(s)(\tilde{x}-1)} - c^{\mathrm{n}}_4(s)\Lambda^{\mathrm{n}}_2(s) e^{-\Lambda^{\mathrm{n}}_2(s)\tilde{x}},\end{aligned}$$

and in the positive electrode to be:

$$\frac{\nabla_{\tilde{x}}\,\widetilde{\Theta}_{\mathrm{e}}^{\mathrm{p}}(\tilde{x},s)}{I_{\mathrm{app}}(s)} = -c_1^{\mathrm{p}}(s)\Lambda_1^{\mathrm{p}}(s)e^{\Lambda_1^{\mathrm{p}}(s)(2-\tilde{x})} + c_2^{\mathrm{p}}(s)\Lambda_1^{\mathrm{p}}(s)e^{-\Lambda_1^{\mathrm{p}}(s)(3-\tilde{x})} - c_3^{\mathrm{p}}(s)\Lambda_2^{\mathrm{p}}(s)e^{\Lambda_2^{\mathrm{p}}(s)(2-\tilde{x})} + c_4^{\mathrm{p}}(s)\Lambda_2^{\mathrm{p}}(s)e^{-\Lambda_2^{\mathrm{p}}(s)(3-\tilde{x})},$$

and finally in the separator to be:

$$\frac{\nabla_{\tilde{x}}\,\widetilde{\Theta}_{\mathrm{e}}^{\mathrm{s}}(\tilde{x},s)}{I_{\mathrm{app}}(s)} = c_1^{\mathrm{s}}(s)\Lambda_1^{\mathrm{s}}(s)e^{\Lambda_1^{\mathrm{s}}(s)(\tilde{x}-2)} - c_2^{\mathrm{s}}(s)\Lambda_1^{\mathrm{s}}(s)e^{-\Lambda_1^{\mathrm{s}}(s)(\tilde{x}-1)}.$$

Gradient TF of electrolyte potential, $\nabla_{\tilde{x}}\phi_{\mathrm{e}}$

- The debiased lumped electrolyte potential was previously defined as $\tilde{\phi}_{\mathrm{e}}(\tilde{x},t) = \phi_{\mathrm{e}}(\tilde{x},t) - \phi_{\mathrm{e},0}(0,t)$.
- Then the gradient we seek to find is:

$$\nabla_{\tilde{x}}\phi_{\mathrm{e}}(\tilde{x},t) = \nabla_{\tilde{x}}\tilde{\phi}_{\mathrm{e}}(\tilde{x},t) + \nabla_{\tilde{x}}\phi_{\mathrm{e},0}(0,t).$$

- Since $\phi_{\mathrm{e},0}(0,t)$ is not dependent on $\tilde{x}$, $\nabla_{\tilde{x}}\phi_{\mathrm{e}}(\tilde{x},t) = \nabla_{\tilde{x}}\tilde{\phi}_{\mathrm{e}}(\tilde{x},t)$.
- To find this gradient, recall that the debiased electrolyte-potential TF in the negative electrode was defined as:

$$\frac{\widetilde{\Phi}_{\mathrm{e}}^{\mathrm{n}}(\tilde{x},s)}{I_{\mathrm{app}}(s)} = \frac{\left[\widetilde{\Phi}_{\mathrm{e}}^{\mathrm{n}}(\tilde{x},s)\right]_1}{I_{\mathrm{app}}(s)} + \frac{\left[\widetilde{\Phi}_{\mathrm{e}}^{\mathrm{n}}(\tilde{x},s)\right]_2}{I_{\mathrm{app}}(s)}. \tag{6.13}$$

Taking the gradient and expressing the final result in terms of $\tilde{x}$ yields:

$$\frac{\nabla_{\tilde{x}}\,\widetilde{\Phi}_{\mathrm{e}}^{\mathrm{n}}(\tilde{x},s)}{I_{\mathrm{app}}(s)} = \frac{\left[\nabla_{\tilde{x}}\,\widetilde{\Phi}_{\mathrm{e}}^{\mathrm{n}}(\tilde{x},s)\right]_1}{I_{\mathrm{app}}(s)} + \frac{\left[\nabla_{\tilde{x}}\,\widetilde{\Phi}_{\mathrm{e}}^{\mathrm{n}}(\tilde{x},s)\right]_2}{I_{\mathrm{app}}(s)},$$

where:

$$\frac{\left[\nabla_{\tilde{x}}\,\widetilde{\Phi}_{\mathrm{e}}^{\mathrm{n}}(\tilde{x},s)\right]_1}{I_{\mathrm{app}}(s)} = -\left(\mathrm{j}_1^{\mathrm{n}}\frac{e^{\Lambda_1^{\mathrm{n}}(\tilde{x}-1)} - e^{-\Lambda_1^{\mathrm{n}}}}{\bar{\kappa}^{\mathrm{n}}\Lambda_1^{\mathrm{n}}} + \mathrm{j}_2^{\mathrm{n}}\frac{-e^{-\Lambda_1^{\mathrm{n}}\tilde{x}} + 1}{\bar{\kappa}^{\mathrm{n}}\Lambda_1^{\mathrm{n}}}\right.$$

$$+ \mathrm{j}_3^{\mathrm{n}} \frac{e^{\Lambda_2^{\mathrm{n}}(\tilde{x}-1)} - e^{-\Lambda_2^{\mathrm{n}}}}{\bar{\kappa}^{\mathrm{n}} \Lambda_2^{\mathrm{n}}} + \mathrm{j}_4^{\mathrm{n}} \frac{-e^{-\Lambda_2^{\mathrm{n}}\tilde{x}} + 1}{\bar{\kappa}^{\mathrm{n}} \Lambda_2^{\mathrm{n}}} \Bigg)$$

$$\frac{\left[\nabla_{\tilde{x}} \widetilde{\Phi}_{\mathrm{e}}^{\mathrm{n}}(\tilde{x}, s)\right]_2}{I_{\mathrm{app}}(s)} = -\bar{\kappa}_D T \left(\Lambda_1^{\mathrm{n}} \left(c_1^{\mathrm{n}} e^{\Lambda_1^{\mathrm{n}}(\tilde{x}-1)} - c_2^{\mathrm{n}} e^{-\Lambda_1^{\mathrm{n}}\tilde{x}} \right) \right.$$

$$\left. + \Lambda_2^{\mathrm{n}} \left(c_3^{\mathrm{n}} e^{\Lambda_2^{\mathrm{n}}(\tilde{x}-1)} - c_4^{\mathrm{n}} e^{-\Lambda_2^{\mathrm{n}}\tilde{x}} \right) \right).$$

- The electrolyte-potential TF for the separator region also has two spatially varying components.
- Taking the gradient of these terms and expressing the overall electrolyte-potential gradient in terms of $\tilde{x}$ yields:

$$\frac{\nabla_{\tilde{x}} \widetilde{\Phi}_{\mathrm{e}}^{\mathrm{s}}(\tilde{x}, s)}{I_{\mathrm{app}}(s)} = -\frac{1}{\bar{\kappa}^{\mathrm{s}}} - \bar{\kappa}_D T \Lambda_1^{\mathrm{s}} \left(c_1^{\mathrm{s}} e^{\Lambda_1^{\mathrm{s}}(\tilde{x}-2)} - c_2^{\mathrm{s}} e^{-\Lambda_1^{\mathrm{s}}(\tilde{x}-1)} \right).$$

- Finally, the electrolyte-potential TF for the positive electrode also has two spatially varying components.
- Taking the gradient of these terms and expressing the overall electrolyte-potential gradient in terms of $\tilde{x}$ yields:

$$\frac{\nabla_{\tilde{x}} \widetilde{\Phi}_{\mathrm{e}}^{\mathrm{p}}(\tilde{x}, s)}{I_{\mathrm{app}}(s)} = \frac{\left[\nabla_{\tilde{x}} \widetilde{\Phi}_{\mathrm{e}}^{\mathrm{p}}(\tilde{x}, s)\right]_1}{I_{\mathrm{app}}(s)} + \frac{\left[\nabla_{\tilde{x}} \widetilde{\Phi}_{\mathrm{e}}^{\mathrm{p}}(\tilde{x}, s)\right]_2}{I_{\mathrm{app}}(s)},$$

where:

$$\frac{\left[\nabla_{\tilde{x}} \widetilde{\Phi}_{\mathrm{e}}^{\mathrm{p}}(\tilde{x}, s)\right]_1}{I_{\mathrm{app}}(s)} = -\frac{1}{\bar{\kappa}^{\mathrm{p}}} + \Bigg(\mathrm{j}_1^{\mathrm{p}} \frac{e^{\Lambda_1^{\mathrm{p}}(2-\tilde{x})} - 1}{\bar{\kappa}^{\mathrm{p}} \Lambda_1^{\mathrm{p}}} + \mathrm{j}_2^{\mathrm{p}} \frac{e^{-\Lambda_1^{\mathrm{p}}} - e^{-\Lambda_1^{\mathrm{p}}(3-\tilde{x})}}{\bar{\kappa}^{\mathrm{p}} \Lambda_1^{\mathrm{p}}} \right.$$

$$\left. + \mathrm{j}_3^{\mathrm{p}} \frac{e^{\Lambda_2^{\mathrm{p}}(2-\tilde{x})} - 1}{\bar{\kappa}^{\mathrm{p}} \Lambda_2^{\mathrm{p}}} + \mathrm{j}_4^{\mathrm{p}} \frac{e^{-\Lambda_2^{\mathrm{p}}} - e^{-\Lambda_2^{\mathrm{p}}(3-\tilde{x})}}{\bar{\kappa}^{\mathrm{p}} \Lambda_2^{\mathrm{p}}} \Bigg),$$

$$\frac{\left[\nabla_{\tilde{x}} \widetilde{\Phi}_{\mathrm{e}}^{\mathrm{p}}(\tilde{x}, s)\right]_2}{I_{\mathrm{app}}(s)} = \bar{\kappa}_D T \left(\Lambda_1^{\mathrm{p}} \left(c_1^{\mathrm{p}} e^{\Lambda_1^{\mathrm{p}}(2-\tilde{x})} - c_2^{\mathrm{p}} e^{-\Lambda_1^{\mathrm{p}}(3-\tilde{x})} \right) \right.$$

$$\left. + \Lambda_2^{\mathrm{p}} \left(c_3^{\mathrm{p}} e^{\Lambda_2^{\mathrm{p}}(2-\tilde{x})} - c_4^{\mathrm{p}} e^{-\Lambda_2^{\mathrm{p}}(3-\tilde{x})} \right) \right).$$

Gradient TF of solid potential, $\nabla_{\tilde{x}}\phi_{\mathrm{s}}$

- The debiased lumped solid potential was previously defined as $\tilde{\phi}_{\mathrm{s}}(\tilde{x},t)=\phi_{\mathrm{s}}(\tilde{x},t)-\phi_{\mathrm{s}}(0,t)$.
- Then, the gradient we seek to find is:

$$\nabla_{\tilde{x}}\phi_{\mathrm{s}}(\tilde{x},t)=\nabla_{\tilde{x}}\tilde{\phi}_{\mathrm{s}}(\tilde{x},t)+\nabla_{\tilde{x}}\phi_{\mathrm{s}}(0,t).$$

  Since $\phi_{\mathrm{s}}(0,t)$ is not dependent on $\tilde{x}$, $\nabla_{\tilde{x}}\phi_{\mathrm{s}}(\tilde{x},t)=\nabla_{\tilde{x}}\tilde{\phi}_{\mathrm{s}}(\tilde{x},t)$.
- The TFs for $\tilde{\phi}_{\mathrm{s}}(\tilde{x},t)$ in the negative and positive electrodes were expressed in Ch. 2 as well.
- Taking the gradient of these TFs, and expressing the final result in terms of $\tilde{x}$ yields:

$$\begin{aligned}\frac{\nabla_{\tilde{x}}\widetilde{\Phi}^{\mathrm{n}}_{\mathrm{s}}(\tilde{x},s)}{I_{\mathrm{app}}(s)}&=-\frac{1}{\bar{\sigma}^{\mathrm{n}}}+\mathrm{j}^{\mathrm{n}}_1\frac{e^{\Lambda^{\mathrm{n}}_1(\tilde{x}-1)}-e^{-\Lambda^{\mathrm{n}}_1}}{\bar{\sigma}^{\mathrm{n}}\Lambda^{\mathrm{n}}_1}+\mathrm{j}^{\mathrm{n}}_2\frac{1-e^{-\Lambda^{\mathrm{n}}_1\tilde{x}}}{\bar{\sigma}^{\mathrm{n}}\Lambda^{\mathrm{n}}_1}\\&\quad+\mathrm{j}^{\mathrm{n}}_3\frac{e^{\Lambda^{\mathrm{n}}_2(\tilde{x}-1)}-e^{-\Lambda^{\mathrm{n}}_2}}{\bar{\sigma}^{\mathrm{n}}\Lambda^{\mathrm{n}}_2}+\mathrm{j}^{\mathrm{n}}_4\frac{1-e^{-\Lambda^{\mathrm{n}}_2\tilde{x}}}{\bar{\sigma}^{\mathrm{n}}\Lambda^{\mathrm{n}}_2}\\\frac{\nabla_{\tilde{x}}\widetilde{\Phi}^{\mathrm{p}}_{\mathrm{s}}(\tilde{x},s)}{I_{\mathrm{app}}(s)}&=-\frac{1}{\bar{\sigma}^{\mathrm{p}}}-\mathrm{j}^{\mathrm{p}}_1\frac{e^{\Lambda^{\mathrm{p}}_1(2-\tilde{x})}-e^{-\Lambda^{\mathrm{p}}_1}}{\bar{\sigma}^{\mathrm{p}}\Lambda^{\mathrm{p}}_1}-\mathrm{j}^{\mathrm{p}}_2\frac{1-e^{-\Lambda^{\mathrm{p}}_1(3-\tilde{x})}}{\bar{\sigma}^{\mathrm{p}}\Lambda^{\mathrm{p}}_1}\\&\quad-\mathrm{j}^{\mathrm{p}}_3\frac{e^{\Lambda^{\mathrm{p}}_2(2-\tilde{x})}-e^{-\Lambda^{\mathrm{p}}_2}}{\bar{\sigma}^{\mathrm{p}}\Lambda^{\mathrm{p}}_2}-\mathrm{j}^{\mathrm{p}}_4\frac{1-e^{-\Lambda^{\mathrm{p}}_2(3-\tilde{x})}}{\bar{\sigma}^{\mathrm{p}}\Lambda^{\mathrm{p}}_2}.\end{aligned}$$